

## Article

# Phosphate Removal Efficiency and Life Cycle Assessment of Different Anode Materials in Electrocoagulation Treatment of Wastewater

Guangpu Li, Bin Zheng, Wenqing Zhang, Qiaona Liu, Mingzheng Li and Haibing Zhang \*

Faculty of Engineering, China University of Petroleum-Beijing at Karamay, Karamay 834000, China; 2021015639@st.cupk.edu.cn (G.L.); 2020015531@st.cupk.edu.cn (B.Z.); 2021015662@st.cupk.edu.cn (W.Z.); 2021015595@st.cupk.edu.cn (Q.L.); 2021015670@st.cupk.edu.cn (M.L.)

\* Correspondence: zhanghaibing@cupk.edu.cn

**Abstract:** The excessive discharge of phosphorus-containing wastewater contributes to eutrophication, posing a serious threat to aquatic ecosystems. Therefore, methods such as electrocoagulation should be utilized to remove phosphorus from wastewater prior to discharging it into a water body. In this study, we aimed to determine the effectiveness of electrocoagulation in treating simulated phosphorus-containing wastewater under different parameters, including anode material (aluminum, iron, and magnesium), electrode distance (ED) (1, 2.5, and 4.5 cm), pH (3, 6, and 9), and current density (CD) (3, 6, and 9 mA/cm<sup>2</sup>). Additionally, three models of phosphate removal, the pseudo-first-order (PFO), pseudo-second-order (PSO), and Behnjady–Modirshahla–Ghanbery (BMG) models, were used to simulate the relationship between phosphate concentration and time in the electrocoagulation process using the three metals for phosphate removal. The experimental results showed that the aluminum system had the highest removal efficiency (90%) when energized for 20 min under a CD of 3 mA/cm<sup>2</sup>, followed by those of the iron (80%) and magnesium (35%) systems. Furthermore, a life cycle assessment (LCA) showed that the aluminum electrode system had a smaller environmental impact than the iron and magnesium electrode systems. Therefore, the aluminum electrode system is suitable for phosphorus removal from wastewater.



**Citation:** Li, G.; Zheng, B.; Zhang, W.; Liu, Q.; Li, M.; Zhang, H. Phosphate Removal Efficiency and Life Cycle Assessment of Different Anode Materials in Electrocoagulation Treatment of Wastewater. *Sustainability* **2024**, *16*, 3836.

<https://doi.org/10.3390/su16093836>

Academic Editor: Agostina Chiavola

Received: 7 March 2024

Revised: 23 April 2024

Accepted: 30 April 2024

Published: 2 May 2024



**Copyright:** © 2024 by the authors. Licensee MDPI, Basel, Switzerland. This article is an open access article distributed under the terms and conditions of the Creative Commons Attribution (CC BY) license (<https://creativecommons.org/licenses/by/4.0/>).

**Keywords:** phosphorus-containing wastewater; electrode materials; electrocoagulation; kinetic analysis; life cycle assessment

## 1. Introduction

Phosphorus is a limiting nutrient for aquatic plants and algae, and the excessive discharge of phosphorus-containing wastewater can easily trigger eutrophication in water bodies [1,2]. Eutrophication is characterized by nutrient enrichment that promotes the overgrowth of algae, leading to hypoxic conditions, dead zones, and the degradation of water quality. Eutrophication leads to substantial changes in the structure and functions of ecosystems, increasing their instability, and it is difficult to reverse. Hence, the damage caused to ecosystems by eutrophication is profound [3]. Slaughterhouse wastewater is a typical phosphorus-containing industrial wastewater, accounting for up to 6% of China's industrial wastewater discharge. It contains animal feces, urine, and blood, of which feces and urine contain large amounts of phosphorus [4,5]. China's National Ministry of Environmental Protection issued a revised version of the Meat Processing Wastewater Discharge Standard (GB 13457-1992) in 2017, which requires that wastewater discharged from slaughterhouses contain no more than 8 mg/L of phosphorus. Therefore, the efficient and effective treatment of phosphorus-containing wastewater is crucial for preventing water pollution, thereby serving as a significant step towards the achievement of the United Nations Sustainable Development Goals (SDGs) pertaining to environmental protection and sustainable development.

At present, there are many technologies that can be used for wastewater treatment [6,7]. Phosphorus can be removed from wastewater using three conventional methods: adsorption, chemical treatment, and activated sludge treatment. Phosphorus is often extracted using adsorption, which has a low secondary pollution rate, easy operation, and high removal efficiency [8]. Phosphate is removed from wastewater during physical adsorption and ion exchange processes. High concentrations of phosphorus-containing solutions can then be used to elute the phosphate. The adsorption of phosphate in water using metal–organic frameworks and modified composite clays has shown good results [9,10]. Phosphates can be adsorbed onto a wide range of composite and modified materials [11–13]. However, these adsorbents have drawbacks, including low phosphate selectivity, limited capacity, substantial acid and base consumption during material production, and performance degradation after repeated cycling [14]. Phosphorus is chemically eliminated via precipitation. The chemical removal of phosphate from wastewater involves the addition of appropriate proportions of precipitating metal salts or minerals [15]. Chemical phosphorus removal can reduce the total content in treated wastewater to less than 1 mg/L [16]. In addition, the chemical residues have the potential for recycling. For example, using magnesium salt for chemical precipitation, high-phosphorus wastewater and sludge return liquid can be converted to ammonium magnesium phosphate, which can then be used as a fertilizer on farms [17]. However, the addition of chemicals to the treatment process results in the formation of flocs and suspended debris, which can lead to secondary pollution. Moreover, dose control is challenging [18]. Phosphorus-aggregating organisms absorb dissolved phosphorus for storage in their bodies and are discharged with the remaining sludge, making the activated sludge method the most widely used wastewater phosphorus removal method. This method primarily removes biological phosphorus from wastewater via activated sludge treatment [19]. Previous studies have used microalgae to remove phosphorus from wastewater [20]. These algae primarily assimilate and absorb phosphorus from the water column [21]. However, environmental factors influence the effectiveness of the activated sludge method, necessitating costly management of the activated sludge in the early stages. Further research is necessary to determine whether microalgae can effectively cleanse industrial wastewater considering the complicated composition of these fluids. Mateus et al. treated slaughterhouse effluent using electrocoagulation with iron and aluminum as anodes in response to the high phosphorus concentration and intermittent wastewater discharge. This process resulted in total phosphorus reductions of approximately 98% and 97% for iron and aluminum, respectively [22,23]. Therefore, electrocoagulation is a promising technology for treating slaughterhouse wastewater.

Electrocoagulation has been used extensively in water treatment owing to its advantages compared to traditional phosphorus removal technology. The advantages include simple equipment, convenient operation, a low cost, high efficiency, and pollutant removal [24]. Using an applied electric field, the electrocoagulation process removes pollutants from the environment by hydrolyzing and polymerizing cations produced in situ at the anode into various polynuclear hydroxyl compatibilities and hydroxides. These compounds exhibit good flocculation, precipitation, and adsorption properties [25].

Many wastewater treatment methods have been implemented using electrocoagulation technology. The most common applications for electrocoagulation include the treatment of heavy metal wastewater [26], leather wastewater [27], oil-containing wastewater [28,29], textile wastewater [30], medical wastewater [31], slaughterhouse wastewater [32–34], and silica-containing wastewater [35,36]. Electrocoagulation is an efficient method for the treatment of a wide range of contaminants. Phosphates can also be effectively removed from wastewater using electrocoagulation. To extract phosphate from household wastewater containing 52.13 mg/L of phosphate, Omwene et al. built an electrocoagulation reactor with a titanium cathode and an aluminum–iron hybridized anode. Under ideal conditions, the reactor achieved 99.99% phosphate removal [37]. Supriya et al. removed 93.94% of phosphorus from simulated wastewater with a starting concentration of 20 mg/L at a pH of 7 and an energization time of 25 min using an iron electrode for electrocoagulation [38].

Dura et al. electroflocculated water samples with an aluminum–magnesium alloy anode and achieved 100% phosphate removal after 15 min of energization [39]. Phosphorus contaminants in wastewater can be successfully removed using electrocoagulation technology; however, anode selection affects cost and removal efficiency. Devlin et al. used magnesium, iron, and aluminum as anodes for electrocoagulation treatment and discovered that the magnesium electrode exhibited poor orthophosphate removal. In contrast, the aluminum and iron electrodes exhibited very high removal rates [40]. Omwene et al. used aluminum and ferrous metals as anodes in electrocoagulation tests and discovered that aluminum anodes required shorter energization times and achieved improved treatment efficiency [41]. Meanwhile, magnesium metal has drawn increasing attention as a potential anode because of the nonrenewable nature of phosphorus [42,43].

Aluminum and iron are two widely used electrode materials for phosphorus removal through electrocoagulation. Magnesium has also received attention from researchers in recent years because of its potential value for phosphorus recovery from wastewater. Currently, there is a lack of comprehensive studies that have evaluated and contrasted the effectiveness of these three metal materials in the electrocoagulation treatment of phosphate in wastewater. Therefore, a life cycle assessment (LCA) must be conducted for a systematic evaluation of the performance of different metals. In this study, we aimed to achieve the following: (1) evaluate the performance of three metal anodes in the electrocoagulation process for treating phosphorus-containing simulated water under different operating parameters and (2) assess the environmental impacts of the process at the midpoint and endpoint through an LCA. This study is the first to conduct a comprehensive and objective LCA of the removal of phosphorus through electrocoagulation and compare the effect of different electrocoagulation materials under the same conditions.

## 2. Materials and Methods

### 2.1. Simulated Wastewater

Phosphorus-containing wastewater that simulated slaughterhouse wastewater was used in this study. The pH and phosphate concentration of the simulated wastewater were based on the properties of wastewater extracted from a slaughterhouse in Xinjiang, China (pH, 7.25; phosphate concentration, 92.7 mg/L). We employed analytical grade NaCl (Sinopharm, Beijing, China) as a supporting electrolyte at a dosage of 1000 mg/L and  $\text{KH}_2\text{PO}_4$  (Innochem, Beijing, China) as a source of phosphorus pollutant for the simulated wastewater at a concentration of 90 mg/L.

### 2.2. Experimental Apparatus and Method for Electrocoagulation

Figure 1 shows the experimental setup. The tests were conducted at intervals of 20 min, with a constant temperature of  $25 \pm 2$  °C. The electrocoagulation device consisted of two electrodes coupled to a DC power source and an electrolyzer with magnetic stirring. The electrocoagulation cell, made of acrylic plates, had a capacity of 900 mL, and the dimensions were  $110 \times 82 \times 140$  mm (length  $\times$  width  $\times$  height). The electrode materials used in the experiments were aluminum, magnesium, and iron. The same materials were used for the cathode and anode. The electrodes measured  $100 \times 100 \times 2$  mm (length  $\times$  width  $\times$  height) and had a parallel area of  $100 \text{ cm}^2$ . Prior to the experiments, the electrodes were polished using sandpaper, cleaned with hydrochloric acid and deionized water, dried, and prepared for subsequent analysis.

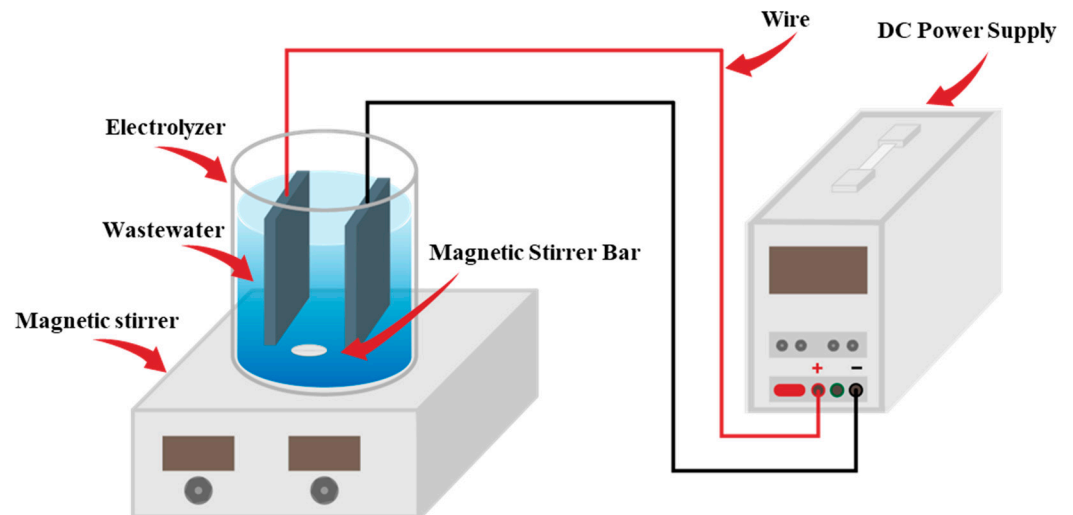
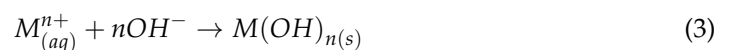


Figure 1. Experimental setup.

In these experiments, the effects of single-factor variations in the electrode distance (ED), initial pH, and current density (CD) on the experimental results were investigated. The initial phosphate concentration was 100 mg/L, and we tested the phosphate removal capacity of the system under different experimental conditions. For example, the initial pH was set to 6.01, the CD was set to 3 mA/cm<sup>2</sup>, and different EDs (1, 2.5, and 4.5 cm) were tested. Alternatively, the ED was set to 2.5 cm, the CD was set to 3 mA/cm<sup>2</sup>, and different initial pH values (3, 6, and 9) were tested. Finally, the ED was set to 2.5 cm, the initial pH was set to 6.01, and different CDs (3, 6, and 9 mA/cm<sup>2</sup>) were tested. In the kinetic tests, samples were obtained from the supernatant every 5 and 10 min under the specified experimental conditions. After filtration, the mass concentration of phosphorus in the solution was calculated using ion chromatography, which was also used to simultaneously measure the voltage, pH, and electrode weight. Each set of tests was run twice in parallel to eliminate the possibility of errors in the experimental results.

Figure 2 shows the principles of electrocoagulation. Following energization, the anode undergoes oxidation and the cathode undergoes reduction. The primary anode (Equation (1)), cathode (Equation (2)), and in-solution (Equation (3)) reactions are as follows:



### 2.3. Sample Analysis and Calculation Methods

Using an ion chromatograph (Dionex Aquion, Waltham, MA, USA), the amount of orthophosphate in the water samples collected for the experiment was determined, and Equation (4) was used to compute the phosphate removal efficiency.

$$\eta = \frac{C_i - C_e}{C_i} \quad (4)$$

$C_i$  represents the initial orthophosphate concentration (mg/L);  $C_e$  represents the post-treatment phosphate concentration (mg/L).

The electrode consumption was calculated from the difference in the mass of the electrode before and after the reaction, as shown in Equation (5), and an analytical balance was used to measure the weight of the electrode.

$$ELC = m - m' \quad (5)$$

$m$  is the mass of the electrode before the experiment (g);  $m'$  is the mass after the experiment (g).

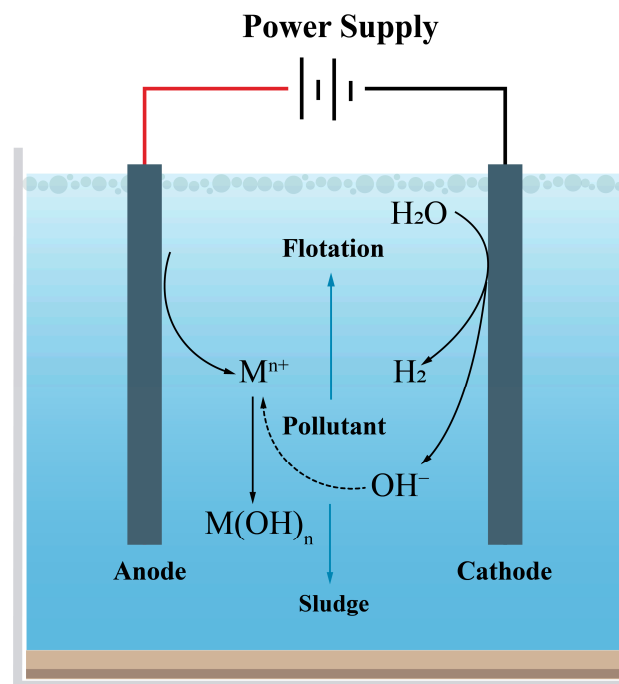


Figure 2. Principle of electrocoagulation.

The energy consumption  $ENC$  (kWh/m<sup>3</sup>) is calculated using Equation (6).

$$ENC = \frac{\sum UIt}{V} \quad (6)$$

$U$  is the voltage (V),  $I$  is the current (A),  $t$  is the electrolysis time (h),  $V$  is the volume of the treated liquid (L), and the voltage is read directly from the DC power supply.

The cost of electricity in Xinjiang, China, is 0.378 CNY/kWh. The treatment cost per liter of wastewater (CNY/L) can be calculated by Equation (7) [44]:

$$Cost = ENC \left( \frac{\sum UIt}{V} \right) * 0.378 \quad (7)$$

The dynamics were investigated using first- and second-order models [45] as well as the BMG model [46]; the first-order model (PFO) was analyzed using Equation (8) as follows:

$$\ln(q_e - q_t) = \ln(q_e) - k_1 t \quad (8)$$

$q_e$  and  $q_t$  are the equilibrium adsorption capacity (mg) and the amount of phosphate adsorbed at time  $t$ , respectively, and  $k_1$  (min<sup>-1</sup>) is the primary reaction rate constant.

The second-order model (PSO) can be calculated using Equation (9):

$$\frac{1}{q_t} * t = \frac{1}{q_e} * 1 + \frac{1}{k_2 q_e^2} \quad (9)$$

$k_2$  (min<sup>-1</sup>) is the second-order reaction rate constant.

The BMG model can be calculated using Equation (10):

$$C_t = \left( 1 - \left[ \frac{t}{m + bt} \right] \right) * C_0 \quad (10)$$

$C_t$  is the concentration of phosphate at moment  $t$  (mg/L),  $C_0$  is the concentration of phosphate at moment  $t = 0$  min (mg/L), and  $t$  is the reaction time (min).  $1/m$  is the phosphate removal rate at the beginning of the process, and  $1/b$  is the theoretical maximum phosphate removal rate.

The pH of the solution at each sampling point was determined by a pH meter (PHS-3E, Shanghai, China). SEM and EDS analyzed Floccs through a scanning electron microscope (Crossbeam 550, Oberkochen, Germany). The composition of the sludge generated by electrocoagulation was analyzed by X-ray diffractometry (D8 Advance, Karlsruhe, Germany), where intensity data were measured over a diffraction angle range from  $5^\circ$  to  $90^\circ$  at a scanning rate of  $2^\circ$  per minute. The main functional groups of the compounds were identified in the  $400\text{--}4000\text{ cm}^{-1}$  range using a Fourier transform infrared spectrometer (FTIR-85, Shanghai, China).

#### 2.4. Life Cycle Assessment

This study employed a comprehensive LCA according to the ISO 14044 standard [47]. This assessment encompasses the following stages: goal and scope definition, life cycle inventory analysis, life cycle impact assessment, life cycle interpretation, and LCA evaluation. We compared the midpoint and endpoint environmental effects of three electrode electrocoagulation treatments for phosphorus-containing wastewater: scenarios 1 (aluminum), 2 (iron), and 3 (magnesium) (Figure 3). See detailed information in the Supplementary Information.

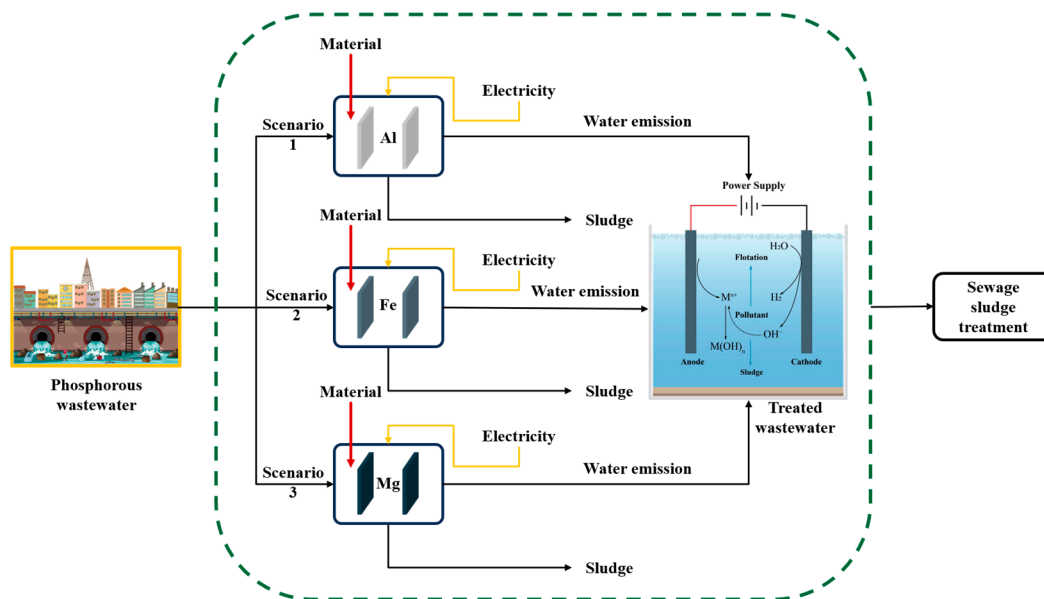


**Figure 3.** System scenarios for wastewater treatment using three anodes: Scenario 1 (aluminum), Scenario 2 (iron), and Scenario 3 (magnesium).

The generated wastewater was treated via electrocoagulation, which was supplied with electricity from the grid and produced treated water and sludge. The three scenarios differed in the use of anode materials.

### 3. Results and Discussion

#### 3.1. Effect of Different Process Conditions

##### 3.1.1. Electrode Distance

The distance between the electrodes affects the resistance generated between the solutions, which, in turn, affects the electrocoagulation removal efficiency [48]. Different EDs (1, 2.5, and 4.5 cm) were investigated to analyze the effect of the three metals as

electrodes on the phosphorus removal efficiency at an initial pH of 6.1 and CD of  $3 \text{ mA/cm}^2$ . The results are shown in Figure 4.

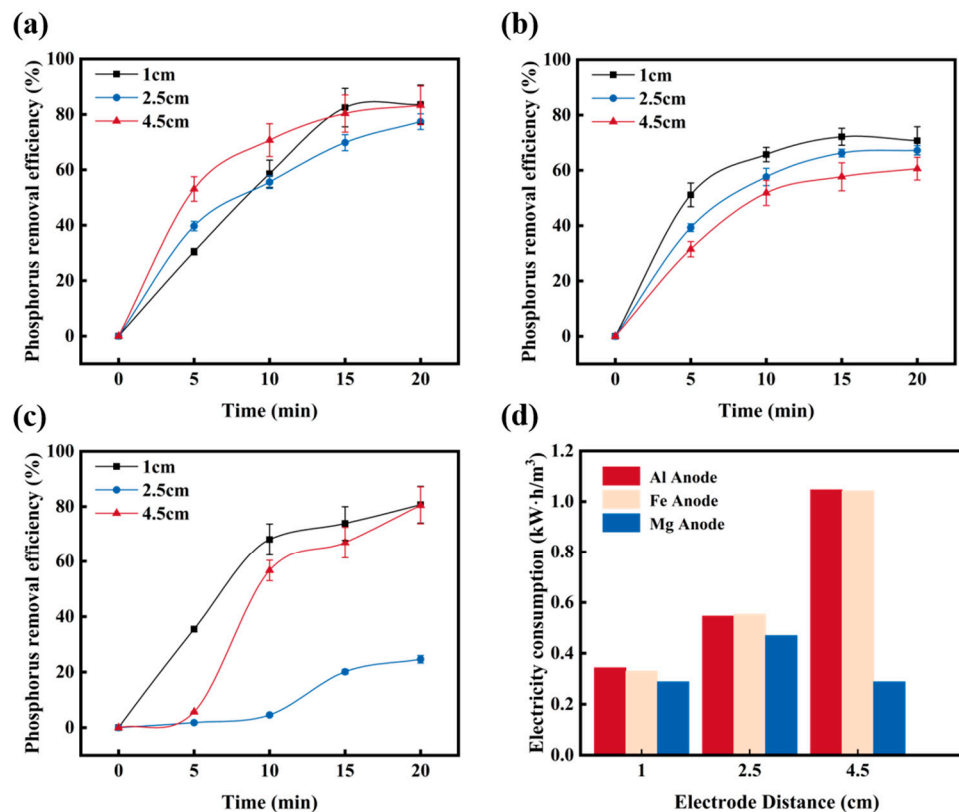


**Figure 4.** Effect of electrode spacing on phosphorus removal from simulated wastewater: (a) aluminum anode, (b) iron anode, (c) magnesium anode, and (d) energy consumption.

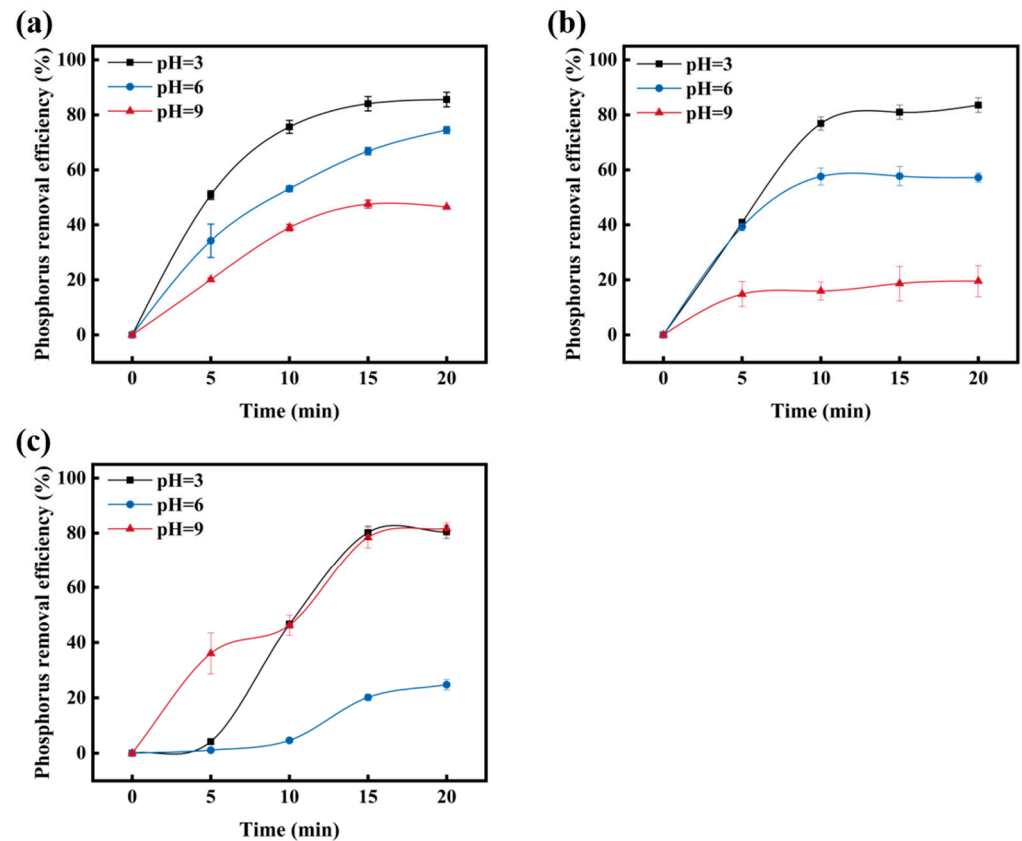
The results indicate that the phosphate removal rate increased as the electrolysis time increased. However, the rate of phosphate removal was higher at EDs of 1 and 4.5 cm than at an ED of 2.5 cm. Figure 4 shows that the removal rates for all three metals were the highest at an ED of 1 cm. The reason for this phenomenon is that the smaller the distance, the stronger the current between the electrodes, which speeds up the electrolysis reaction and produces abundant flocs and bubbles, quickly leading to a very high phosphate removal rate. However, as the ED increases, the current between the electrodes weakens, slowing the release of metal ions between the cathode and anode, and the bubbles generated at the cathode destabilize the anodic floc. This results in weak flocculation, which indirectly leads to a decrease in the phosphate removal rate [45,49].

Figure 4a,c show that the anode floc stability gradually improved with increasing ED; however, the flocculation effect was essentially steady, and the energy consumption also increased. Consequently, an appropriate distance between the electrodes facilitates the mutual synergistic effects of air flotation and flocculation. The bubbles produced by the cathode obstructed the electrode reaction of the oxides away from the anode, thereby facilitating further dissolution of the aluminum electrode and indirectly reinforcing the flocculation effect.

Comprehensive experimental data demonstrated that the magnesium and aluminum electrodes at EDs of 1, 2.5, and 4.5 cm exhibited the phenomenon described above. In contrast, iron electrodes need to be placed at an ED greater than 4.5 cm to achieve mutual synergies of air flotation and flocculation, which will improve the results [49].

### 3.1.2. Initial pH

The initial pH is an operating parameter that affects phosphorus removal through electrocoagulation because it affects the dissolution of anode and cathode metals and the hydration of metal ions in solution to form hydroxides [50]. Three metals were used as electrodes, and their effects were analyzed under different initial pH values (3, 6, and 9) at an ED of 2.5 cm and a CD of 3 mA/cm<sup>2</sup>. Figure 5 shows how varying the starting pH affected the phosphorus removal efficiency of the electrocoagulation process.



**Figure 5.** Effect of initial pH on phosphorus removal from simulated wastewater: (a) aluminum anode, (b) iron anode, and (c) magnesium anode.

As shown in Figure 5a, phosphate removal using the aluminum anode peaked at 87% at a pH of 3 after 20 min of energization, and as the pH increased, phosphate removal steadily dropped after 20 min. This could be because aluminum ions and phosphate are primarily present as  $\text{AlPO}_4$  at the acidic pH of 3. This outcome is consistent with the initial pH of 3 proposed by Attour et al. [51], which is advantageous for phosphate removal kinetics. Additionally, when the pH rises, phosphate and aluminum hydroxide compete for adsorption and precipitation, and because adsorption kinetics are slower than precipitation kinetics, phosphorus removal is hindered owing to a decrease in  $\text{AlPO}_4$  and  $\text{Al}(\text{OH})_3$  generation.

Figure 6a illustrates how the pH changed with the treatment. Initially, the pH was between 3 and 9, but as electrolysis proceeded and  $\text{OH}^-$  was generated at the cathode, the pH progressively increased to 10, which is nearly equal to the pH of the buffer solution in which the  $\text{AlPO}_4/\text{Al}(\text{OH})_3$  mixture forms [52]. As the pH increased, the aluminum hydroxide levels also increased. This caused precipitation on the anode surface, which passivated the electrode plate and increased the voltage and energy consumption [53]. Therefore, a lower initial pH is desirable in terms of efficiency and sustainability, and phosphate removal efficiency was higher at a pH of 6. This makes the industrialization of

electrocoagulation very promising because efficient phosphate removal can be performed without adjusting the initial pH.

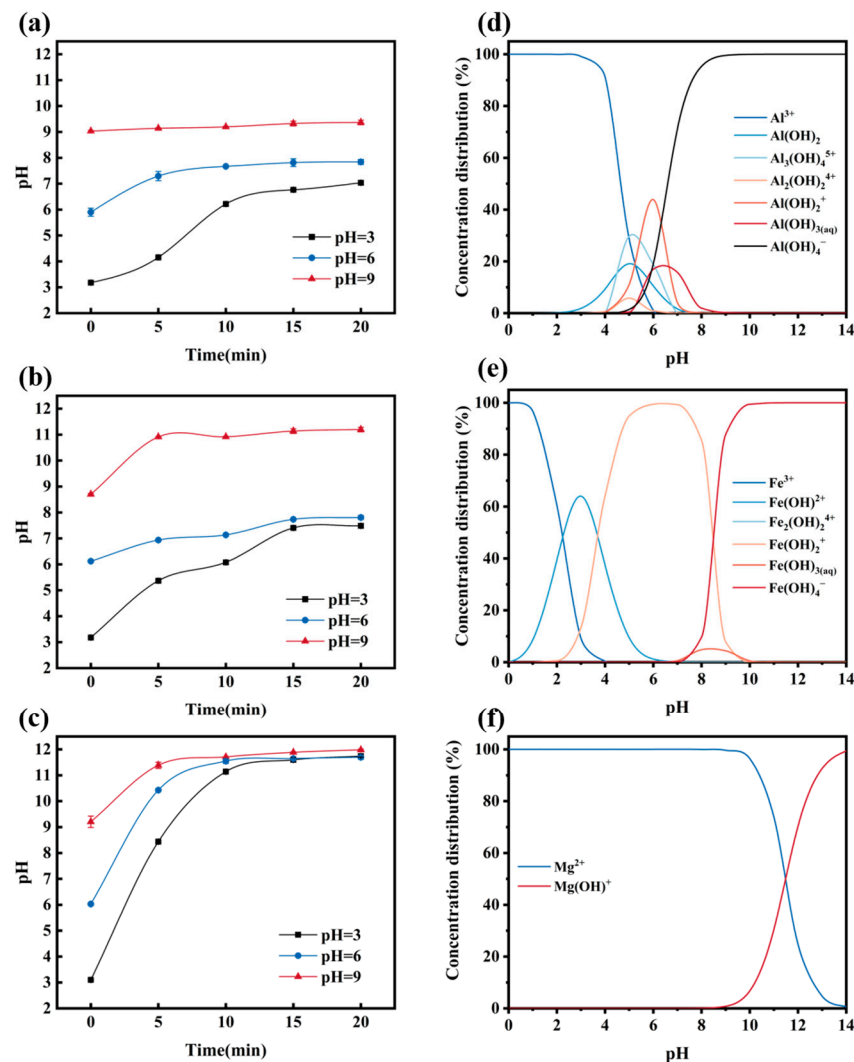


**Figure 6.** Variations in solution pH with time: (a) aluminum, (b) iron, and (c) magnesium. Morphological distribution of substances at different pH values: (d) aluminum, (e) iron, and (f) magnesium.

As shown in Figure 5b, the highest phosphate removal rate using iron as an anode was achieved at an initial pH of 3. After being energized for 20 min, the phosphate removal through iron electrocoagulation was 83% at a pH of 3, 57% at a pH of 6, and 20% at a pH of 9.

Phosphate is often eliminated by  $Fe^{3+}$  when iron is used as the anode, and based on experimental findings, a pH of 3 is ideal. As  $FePO_4$  is less soluble in low-pH solutions, as demonstrated in Figure 6e, phosphate can be eliminated more readily in environments with a lower pH. Upon examining the experimental outcomes under different initial pH values, as illustrated in Figure 5b, it is evident that iron reached its plateau period within 10–15 min. The solubility of  $FePO_4$  increased along with the pH, which reached 7–11 in the solutions depicted in Figure 6b,e. Phosphate removal shifted from precipitation to adsorption, at which point phosphate removal was mainly generated by the adsorption of  $Fe(OH)^{2+}$  and  $Fe(OH)_3$  as well as  $Fe(OH)_4^-$  in solution at a rate lower than the precipitation rate [41]. Therefore, it can be concluded that during electrocoagulation with iron as an anode, phosphate is removed mainly by the production of  $FePO_4$  and adsorption by  $Fe(OH)_3$ ,  $FePO_4$  production tends to favor lower pH values, and a lower initial pH is favorable.

As shown in Figure 5c, the highest phosphate removal rate using magnesium as an anode was greater than 80%. The final removal efficiency was higher at pH values of 3 and 9, whereas at a pH of 6, the removal was less than 14%.

The solution initially contained a large amount of  $H^+$  when the pH was 3, and most of the magnesium was present as  $Mg^{2+}$ . Eventually,  $Mg^{2+}$  precipitated with phosphate to remove it, as shown in Figure 6c,f. The pH of the solution progressively rose to 11.71 as electrolysis continued,  $Mg^{2+}$  increasingly mixed with  $OH^-$ , and the rate of phosphate removal reached the plateau phase. Additionally, the treatment impact was substantially lessened when the initial pH was 6 compared to the impact when the initial pH was 3. The lower phosphate removal rate may have been caused by the competitive relationship between  $OH^-$  and phosphate, and the dominance of  $Mg(OH)^+$  and  $Mg(OH)_2$  formation by  $Mg^{2+}$  and  $OH^-$  in the solution. Additionally, the solution's  $Mg^{2+}$  content gradually decreased, inhibiting the precipitation process of  $Mg^{2+}$  and phosphate. As the pH gradually increased,  $Mg(OH)_2$  and  $Mg(OH)^+$  removed phosphate through adsorption, and the removal rate gradually increased. The solution was alkaline and contained more  $OH^-$  at an initial pH of 9. The  $Mg^{2+}$  produced from electrolysis and the  $OH^-$  in the solution quickly formed hydroxides such as  $Mg(OH)^+$ , and phosphate was then removed through adsorption. As a result, the maximum phosphate removal rate under a pH of 9 was substantially higher compared to that under a pH of 6 and was comparable to that under an initial pH of 3. Consequently, neutral and mildly acidic environments are not ideal when using magnesium as an anode.

Therefore, when treating wastewater containing phosphorus, it is recommended that magnesium electrodes are not used in neutral environments and that aluminum and iron electrodes are utilized in acidic environments.

### 3.1.3. Current Density

Current density is one of the most critical parameters in the process of electrocoagulation, and it dominates anode dissolution, bubble generation between the electrodes, floc growth, pH change, and energy consumption in the treatment process. The higher the CD, the greater the amount of metal ions produced in the solution. However, an excessively high CD tends to passivate the electrodes; therefore, we explored the effect of different CDs (3, 6, and 9  $mA/cm^2$ ) at an ED of 2.5 cm and a pH of 6.01 on the removal of phosphorus from simulated wastewater through electrocoagulation (Figure 7).

As shown in Figure 7a, the removal rate with aluminum as the anode reached 75.36% at 3  $mA/cm^2$ , and the plateau period was not reached at this time. In addition, as the CD increased, the phosphorus removal efficiency increased, reaching nearly 90% at 6 and 9  $mA/cm^2$ , marking the beginning of the plateau period. Thus, when the CD increased, the plateau period progressed.

As shown in Figure 7b, the iron electrode exhibited an earlier plateau than the aluminum electrode at a CD of 3  $mA/cm^2$ . The phosphorus removal efficiency of the iron electrode followed the same pattern as that of the aluminum electrode, with the highest phosphorus removal efficiency of 79.79% at 9  $mA/cm^2$ , followed by that at 6  $mA/cm^2$  (74.19%) and 3  $mA/cm^2$  (51.09%).

The optimal phosphorus removal efficiency of the magnesium electrode after 20 min was 80.73%, as shown in Figure 7c. This was comparable to the efficiency of the iron electrode, although a clear plateau phase was not observed. Notably, the phosphorus removal efficiency of the magnesium electrode was negligible at 3  $mA/cm^2$  and only reached 17.93%. However, as the CD increased to 6  $mA/cm^2$ , the efficiency increased to 75.49%. At the lowest CD, the improvement in phosphorus removal efficiency was not evident in the first 10 min. It can be seen that a higher CD is necessary for a magnesium electrode to achieve a higher phosphorus removal efficiency [54].

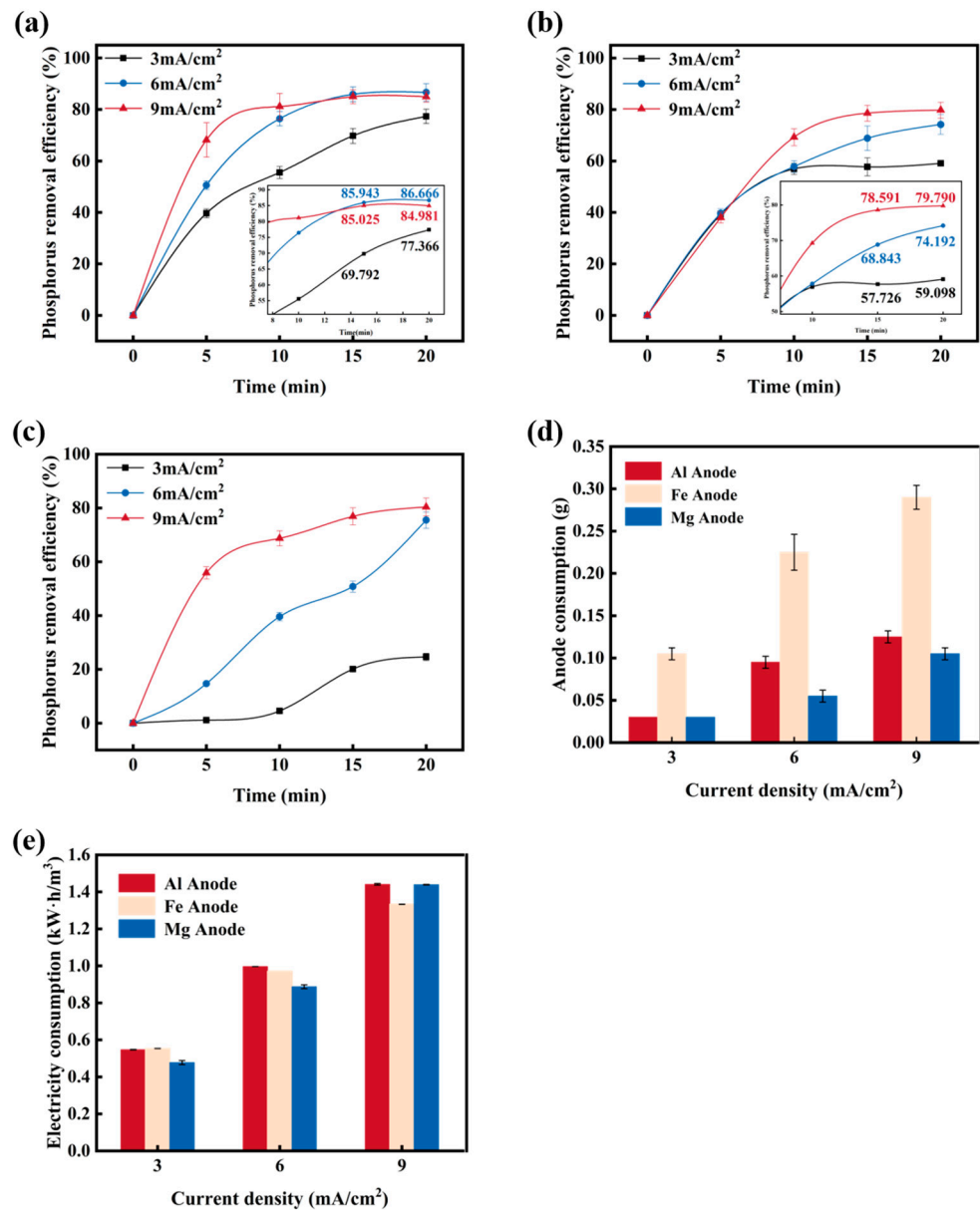


**Figure 7.** Effect of current density on the removal of phosphorus from simulated wastewater: (a) aluminum anode, (b) iron anode, (c) magnesium anode, (d) anode loss, and (e) energy consumption.

The consumption of the iron electrodes was the highest among the three metals, as shown in Figure 7d. The consumption of magnesium and aluminum electrodes was similar, indicating that, to achieve the same phosphorus removal efficiency, the consumption of magnesium and aluminum electrodes was substantially lower than that of iron.

As shown in Figure 7e, the energy consumption of the three metal anodes increased with the increase of CD; the magnesium electrode had the lowest energy consumption, whereas aluminum and iron had a similar energy consumption at 9 mA/cm<sup>2</sup>. In addition, aluminum electrodes had a higher phosphorus removal rate than magnesium electrodes. By comparing the phosphorus removal efficiencies of the three electrodes at 6 and 9 mA/cm<sup>2</sup>, it was discovered that while the energy consumption increased substantially, the phosphorus removal efficiency did not improve substantially with increasing CD. Therefore, a CD of 6 mA/cm<sup>2</sup> is recommended.

An extensive analysis of the above data revealed that the aluminum electrode achieved the highest phosphorus removal efficiency in 20 min. The iron and magnesium electrodes had similar effects, but the iron electrode experienced more substantial loss, and the cost of

the magnesium electrode was considerably higher than that of the iron electrode. Therefore, the most practical and cost-effective CD is  $6 \text{ mA/cm}^2$ , and aluminum is the recommended electrode material [55].

### 3.1.4. Sludge Analysis

After electrocoagulation treatment using three different metals, the dried sludge was characterized using scanning electron microscopy (SEM) and energy-dispersive X-ray spectroscopy (EDS). The color of the sludge generated using aluminum as the electrode in electrocoagulation was off-white, whereas the color of the sludge generated using iron as the electrode was reddish brown, and the color of the sludge generated using magnesium as the electrode was white. Figure 8 shows the findings of the SEM investigation of the flocs produced using the three metals to remove phosphorus from simulated wastewater. Figure 8a,c show that the flocs obtained from the reaction of the aluminum and magnesium electrodes formed many grooves, which could be active sites for flocculation and phosphorus removal. The sludge obtained from the reaction of the magnesium electrode had crumbly nanoparticles on its surface, whereas the sludge obtained from the reaction of the iron electrode had a granular surface, as shown in Figure 8b.

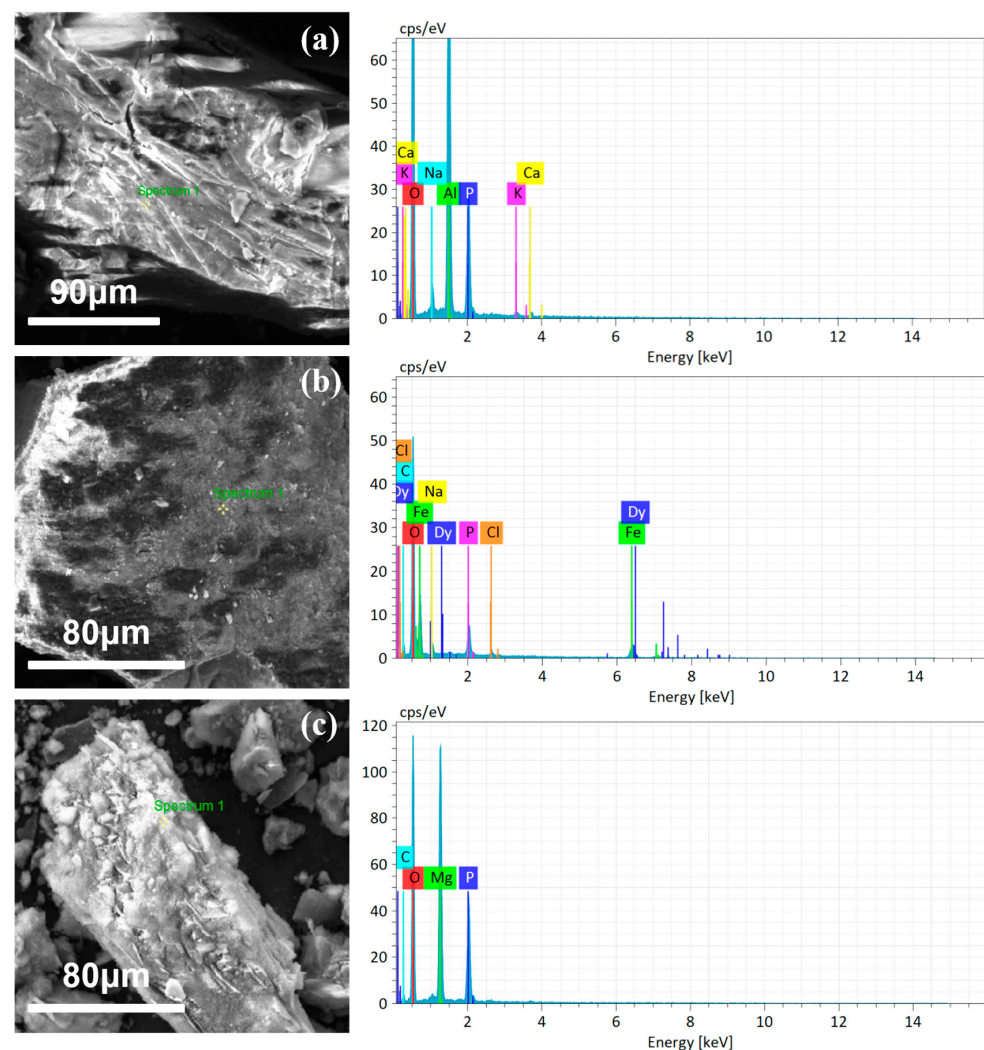


**Figure 8.** Scanning electron microscopy (SEM) and energy-dispersive X-ray spectroscopy (EDS) analysis of the floc generated after electrocoagulation treatment using (a) aluminum, (b) iron, and (c) magnesium.

The presence of phosphorus peaks in the sludge formed from electrocoagulation using the three different types of electrodes is shown in the EDS spectra of the sludge (Figure 8). This indicates that phosphorus was successfully removed from the simulated wastewater.

Figure 8a shows the EDS spectrum of sludge generated using an aluminum electrode and reveals peaks of calcium, potassium, oxygen, sodium, aluminum, and phosphorus, where the presence of elemental aluminum and oxygen was evident, indicating the production of hydroxide roots in the reaction and dissolution of the anode aluminum electrode. Additionally, the presence of oxygen, sodium, and potassium is attributable to the use of  $\text{KH}_2\text{PO}_4$  and  $\text{NaCl}$  in configuring the water samples. Elemental calcium may originate from the hardness of the water. The EDS results indicate that aluminum, oxygen, and phosphorus were present and were major elements in the flocs generated using aluminum electrodes.

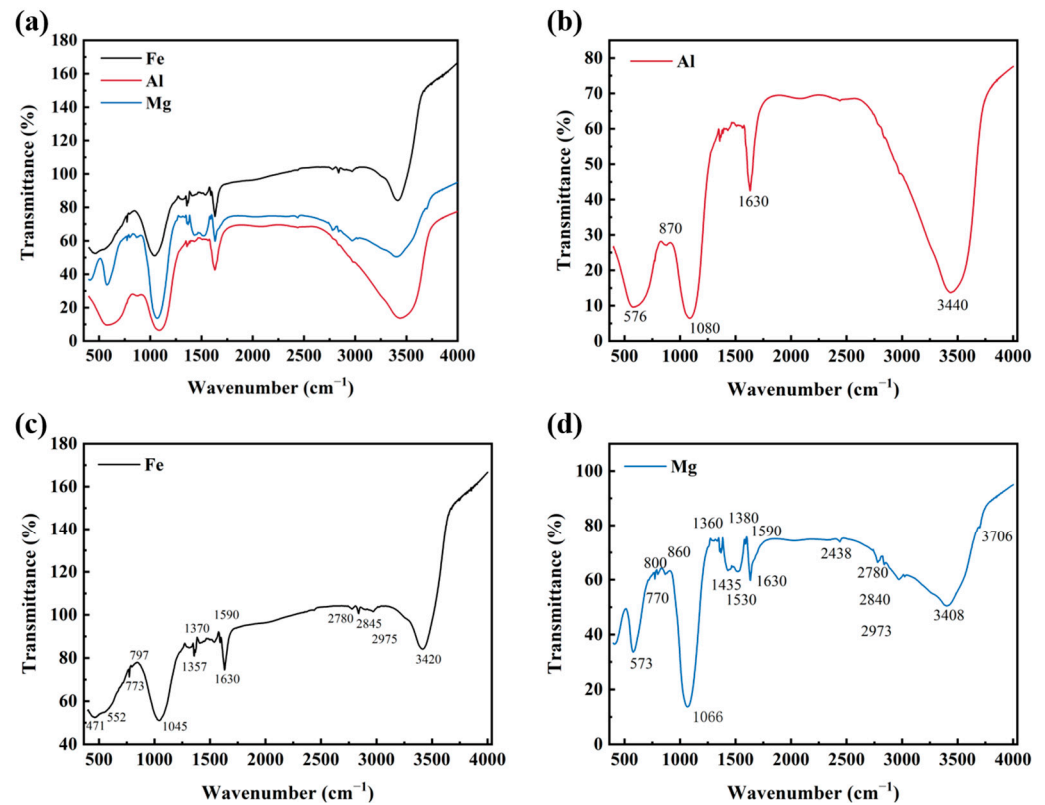
Figure 8b shows the EDS spectrum of electrocoagulation using iron electrodes and reveals peaks of chlorine, carbon, oxygen, sodium, iron, and phosphorus. The presence of iron and oxygen is prominent, and the reason for the presence of chlorine, oxygen, and sodium is similar to that when using the aluminum electrode. The presence of carbon is due to the coke carbon remaining in the iron electrode due to the smelting process in the water. The EDS results show that electrocoagulation using the iron electrode generated iron, oxygen, and phosphorus, which were the main elements present in the flocs.

Figure 8c shows the EDS spectrum of electrocoagulation using magnesium electrodes and reveals peaks of carbon, oxygen, magnesium, and phosphorus, similar to those obtained using aluminum and iron, where the presence of elemental magnesium and oxygen was evident. The presence of elemental carbon likely contributed to the production of magnesium carbonate. The EDS results indicate the presence of magnesium, oxygen, and phosphorus in the floc generated using the magnesium electrode, which were the main elements.

Fourier transform infrared (FT-IR) spectroscopy was used to study the chemical structure of the prepared materials (the sludges). The infrared spectrum of hydroxyapatite shows typical characteristic bands of calcium phosphate in the range of  $400\text{--}4000\text{ cm}^{-1}$ .

As shown in Figure 9, the FT-IR results showed several typical characteristic peaks: the infrared (IR) absorption bands of  $\text{-OH}$  appeared at  $3420\text{ cm}^{-1}$  (stretching) and  $634\text{ cm}^{-1}$  (vibration); the IR absorption peaks at 2940 and 3060 were attributed to  $\nu(\text{CH}_2)$ ; the absorption peak at  $1630\text{ cm}^{-1}$  was due to the adsorption of water on the surface of the material; and the strong IR absorption bands at 1094 and  $1045\text{ cm}^{-1}$  were attributed to the asymmetric stretching ( $\nu_3\text{ PO}_4^{3-}$ ) of phosphate. The IR absorption band at  $962\text{ cm}^{-1}$  was attributed to the symmetric stretching of phosphate ( $\nu_1\text{ PO}_4^{3-}$ ), and the IR absorption bands at  $560\text{--}610\text{ cm}^{-1}$  and  $479\text{ cm}^{-1}$  were attributed to  $\nu_4\text{ PO}_4^{3-}$  and  $\nu_2\text{ PO}_4^{3-}$ , respectively. The absorption bands between  $1459$  and  $1413\text{ cm}^{-1}$  were attributed to the asymmetric stretching of the  $\nu_3\text{ CO}_3^{2-}$  group. This may be related to the low number of carbonate species in the material. Thus, the IR spectra confirmed the presence of phosphate and hydroxyl groups in the sludges.

The sludge generated after phosphorus removal from wastewater through electrocoagulation using three different metal electrodes was analyzed using X-ray diffraction (XRD). As shown in Figure 10, the morphological properties and texture of the sludge produced using the aluminum and iron electrodes indicated that the sludge contained both crystalline and amorphous compounds. The sludge contained hydroxides as the aluminum and iron electrodes dissolved and flocculated the contaminants. A noticeable increase in intensity can be seen at approximately  $20^\circ$ , suggesting that the trivalent iron and aluminum hydroxide sludges were amorphous. However, the analysis of the XRD pattern of the sludge obtained using magnesium electrodes revealed a marked output signal with distinct peaks, indicating the presence of magnesium phosphate hydrate in the sludge.



**Figure 9.** Fourier transform infrared (FT-IR) spectroscopy analysis of the floc generated after electrocoagulation treatment using (a) three metals, (b) aluminum, (c) iron, and (d) magnesium.

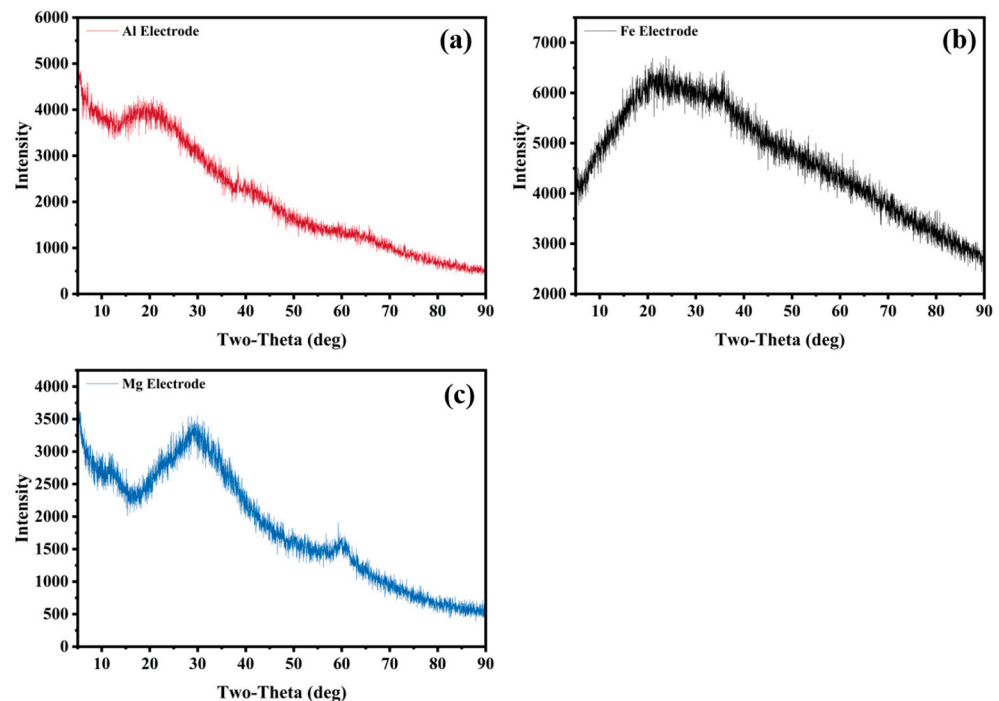


**Figure 10.** X-ray diffraction (XRD) analysis of the floc generated after electrocoagulation treatment using (a) aluminum, (b) iron, and (c) magnesium.

We concluded that the sludge generated from electrocoagulation using aluminum electrodes contained amorphous aluminum phosphate and hydroxy aluminum phosphate, the sludge generated using iron electrodes contained iron phosphate and hydroxyferric phosphate, and that obtained using magnesium electrodes contained magnesium phos-

phate hydrate. These results support the validity of electrocoagulation using electrodes made of these three metals [41].

### 3.2. Operating Costs

The cost of a wastewater treatment system is a crucial factor. Materials (primarily electrodes), energy (mainly electricity), and other costs (e.g., personnel, maintenance, sludge dewatering, and disposal) all affect the total operating expenses, and the main expenditures included in this analysis include energy expenditures (operating costs) and electrode materials (capital costs). After a prolonged experiment simulating the conditions of slaughterhouse wastewater (pH = 6) using a low CD (3 mA/cm<sup>2</sup>) and moderate ED (2.5 cm), the estimated distribution of electrode-related costs was derived as follows: aluminum electrode, 18.45 CNY/kg; iron electrode, 4.06 CNY/kg; and magnesium electrode, 22.9 CNY/kg. The energy consumption costs of using aluminum, iron, and magnesium electrodes were 0.111 CNY/m<sup>3</sup>, 0.107 CNY/m<sup>3</sup>, and 0.0933 CNY/m<sup>3</sup>, respectively. As shown in Figure 11, increasing the treatment time from 20 to 60 min increased the phosphorus removal efficiency by 8%, 21%, and 57% when using aluminum, iron, and magnesium, respectively, while the corresponding increases in the associated costs were 297%, 289%, and 290%, respectively. These values show that a 20 min electrolysis period is the most practical [41] and cost-effective when using aluminum and iron electrodes. Meanwhile, longer energization times are required to improve phosphate removal when using magnesium electrodes. This is related to the removal efficiency and the associated operating costs.

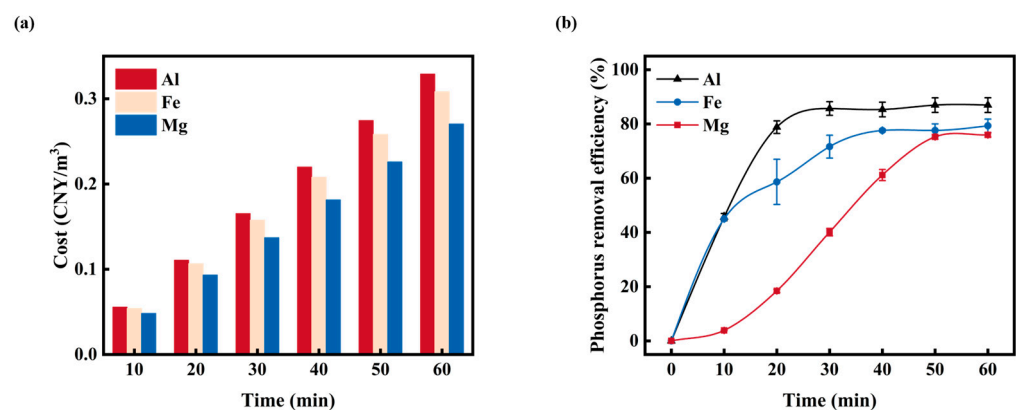


**Figure 11.** Energy consumption and phosphate removal efficiency: (a) electricity consumption vs. energization time and (b) phosphate removal efficiency vs. energization time.

### 3.3. Kinetic Analysis

Understanding the adsorption kinetics and how they are affected by the composition of the aqueous solution is crucial for designing a reactor for the electrocoagulation process. In addition, understanding the adsorption mechanism can help identify the underlying mechanisms that control the adsorption rate. As a result, kinetic studies were carried out to examine the mechanism and the degree to which the three electrode materials fit various kinetic models: PFO, PSO and BMG models. The BMG model is obtained through the mathematical discretization of the secondary adsorption equations, which identify the two main steps that determine the pollutant removal rate: floc generation (Equation (1)) and adsorption of pollutants on the flocs (Equation (3)) [56].

From Table 1, it can be concluded that phosphorus removal using magnesium and iron was most consistent with the second-order level ( $R^2 > 0.98$ ), and that using aluminum was consistent with the first-order level. These values indicated that the removal of total phosphorus from the wastewater using magnesium and aluminum primarily depended on chemisorption. In contrast, the removal of total phosphorus from wastewater using iron primarily depended on physisorption [57]. For the BMG model, aluminum and iron

were fitted to a higher degree and described the two phases of electrocoagulation well. In comparison, magnesium was held at a lower degree because there was insufficient release of  $Mg^{2+}$  at lower CDs, and insufficient  $Mg(OH)_2$  was produced to represent the two phases of electrocoagulation (Figure 12).

**Table 1.** Analysis of kinetic data.

Electrode Material	PFO		PSO		BMG	
	$k_1$	$R^2$	$k_2$	$R^2$	b	$R^2$
Al	0.08583	0.98505	0.00106	0.96771	1.128	0.97864
Fe	0.09259	0.99862	0.0014	0.99149	1.24892	0.98454
Mg	-0.00387	0.94607	$2.97 \times 10^{-6}$	0.94591	1.18849	0.70312

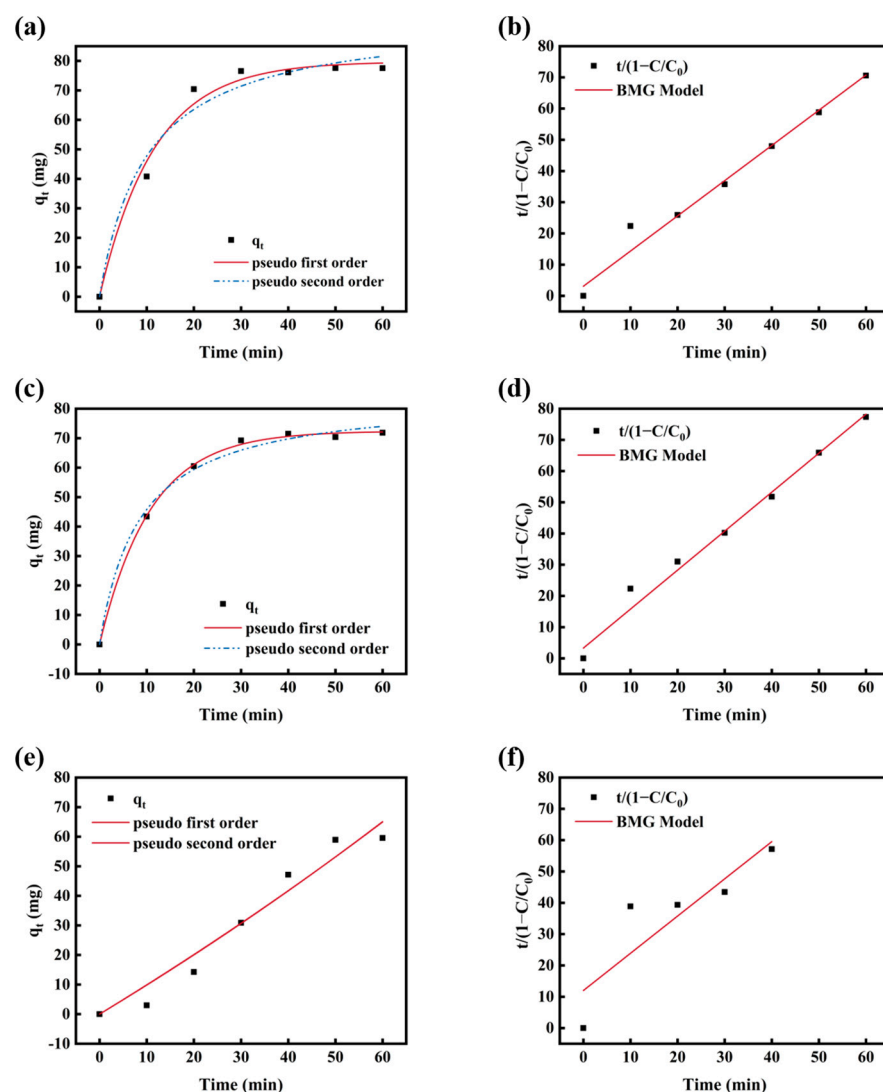


**Figure 12.** Kinetic analyses: (a,b) aluminum, (c,d) iron, and (e,f) magnesium.

### 3.4. Life Cycle Assessment of Electrocoagulation Using Different Electrodes

#### 3.4.1. Life Cycle Assessment

The material energy inputs and outputs of the electrocoagulation system in three scenarios are summarized in Table 2. Electrocoagulation primarily consumes electricity and electrode material.

**Table 2.** Material energy inputs and outputs of sewage treatment.

Inventory Item	Unit	Scenario 1 (Al)	Scenario 2 (Fe)	Scenario 3 (Mg)	Data Quality
<b>Inputs</b>					
Wastewater	m <sup>3</sup>	1	1	1	Experimental
Electricity	kWh	0.5463	0.5534	0.4697	Experimental
Anodic electrode material	kg	0.0375	0.1375	0.0375	Experimental
<b>Outputs</b>					
Treated wastewater	m <sup>3</sup>	1	1	1	Experimental
Sludge	g	223.75	397.50	187.50	Experimental
Product	g	18.75	23.75	16.25	Experimental

Figure 13 shows the environmental impacts of electrocoagulation using the three metals on different indicators. See detailed information in Supplementary Information. The choice of electrode material cannot be based solely on the performance of this material in wastewater treatment. As shown in Figure 13, magnesium is not suitable as an anode material for electrocoagulation, not only because of its poor phosphorus removal efficiency but also because of its high contribution to all midpoint indicators, except for freshwater ecotoxicity. The effects of magnesium can be observed in water softness and problems with human health and safety. A body of water's Mg<sup>2+</sup> content directly influences its softness, which can lead to issues such as pipe scaling [58]. Magnesium is essential for regulating cardiac activity; however, excessive magnesium intake is often accompanied by gastrointestinal reactions, such as nausea and cramps, lethargy, muscle weakness, weak knee-tendon reflexes, and muscle paralysis, whereas complete heart block or cardiac arrest may occur with severe magnesium deficiency [59]. Magnesium reacts readily with water, has a strong affinity for oxygen, is combustible and explosive, and must be stored in a dry atmosphere and transported in a cooling system because of its challenging storage requirements [60].

For the iron electrode, its application environment is more demanding; neutral and alkaline conditions can easily lead to anode passivation, which only applies to the acidic environment, once the passivation needs a high concentration of nitric acid irreversible, it will cause irreversible damage to the environment [60]. However, the prolonged exposure of iron to the air, such as during device shutdown or idling of the equipment accessories, will generate Fe<sup>2+</sup> and Fe<sup>3+</sup>, causing atmospheric corrosion and generating rust, thereby affecting the service life and aggravating the burden of cleanup. In the human body, excessive iron intake destroys liver cells and causes the death of stem cells, leading to the formation of secondary hepatic fibrosis [59]. In the surrounding environment, a large amount of Fe<sup>3+</sup> overflow causes salinization of the surrounding land, restricting the development of crops and affecting food production. For example, Fe<sup>3+</sup> is absorbed by plants, hindering the root system from absorbing nutrients.

Electrocoagulation using aluminum has fewer environmental impacts than that using iron and magnesium, except for its impact on ionizing radiation. These midpoint impact indicators represent water quality, human life, and human health and are commonly used in LCAs of wastewater treatment.

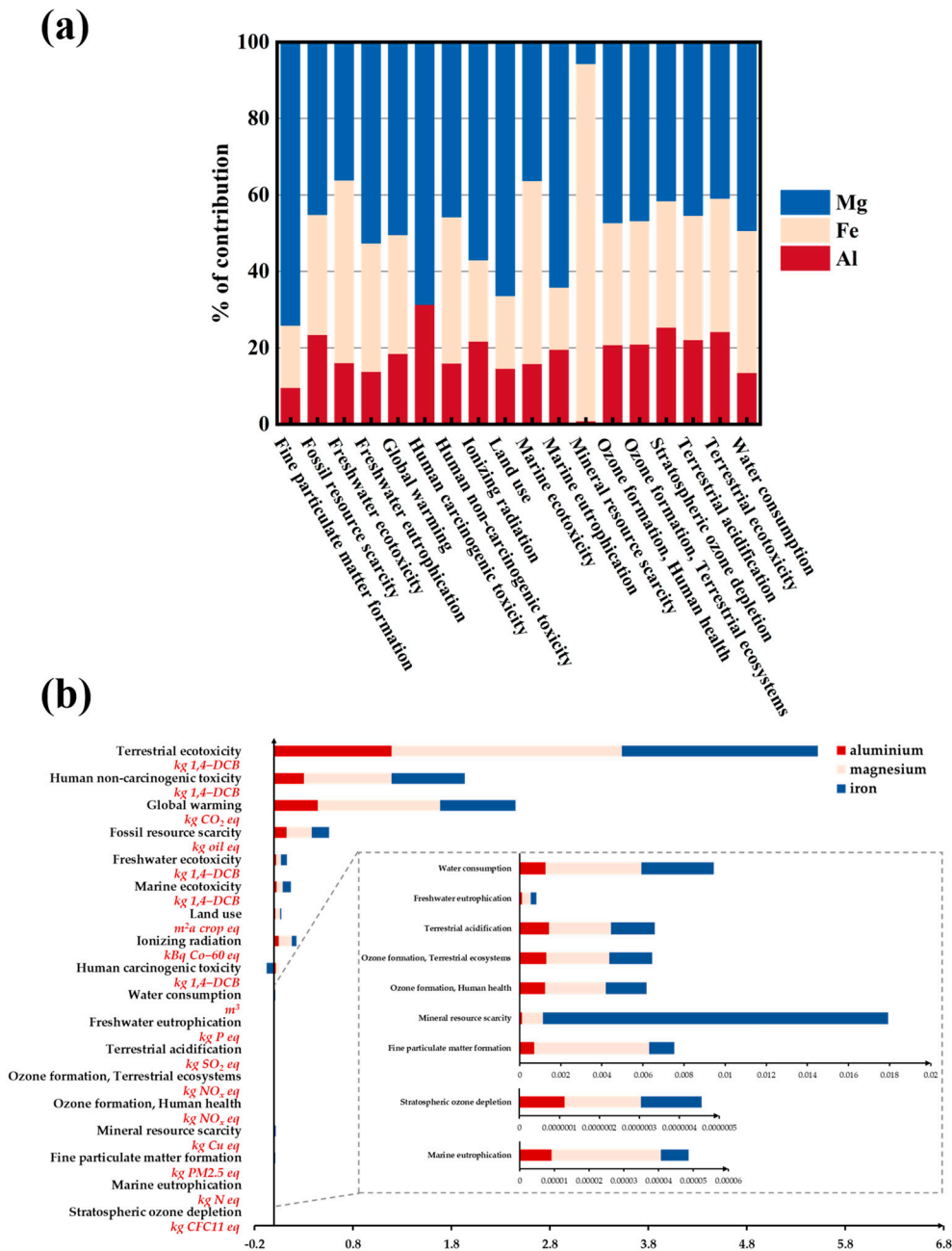


**Figure 13.** Analysis of the contribution of midpoint environmental impact indicators based on all scenarios: (a) results in percentages; (b) results in real values.

Among the impact indicators assessed in this study, global warming, human non-carcinogenic toxicity, and terrestrial ecotoxicity were the most affected. It should be noted that this assessment focused on the operational phase of the treatment process, and that additional impacts may occur during the construction phase. Electricity usage is a major contributor to global warming due to the carbon dioxide produced from burning fossil fuels, and global warming may have harmful effects on water resources [61,62]. Terrestrial ecotoxicity is caused by material consumption during electrode manufacturing. Heavy metals can harm human cells and cause tumors and neurological problems [63,64]. However, the final water discharge and consumption of the electrode materials during electrocoagulation are not carcinogenic to humans. The toxicity of heavy metals directly affects their danger to humans [65,66]. The results of the present study are consistent with those of previous studies.

As shown in Figure 14, the endpoint assessment indicated that electrocoagulation using iron electrodes contributed the most to human health indicators. In terms of ecosystem quality and natural resources, that using iron had the greatest contribution, that using magnesium had the second-largest contribution, and that using aluminum had the lowest contribution. Thus, it can be said that, in this specific instance, the anode material—rather than the wastewater quality—harms the ecosystem and its resources [67,68].

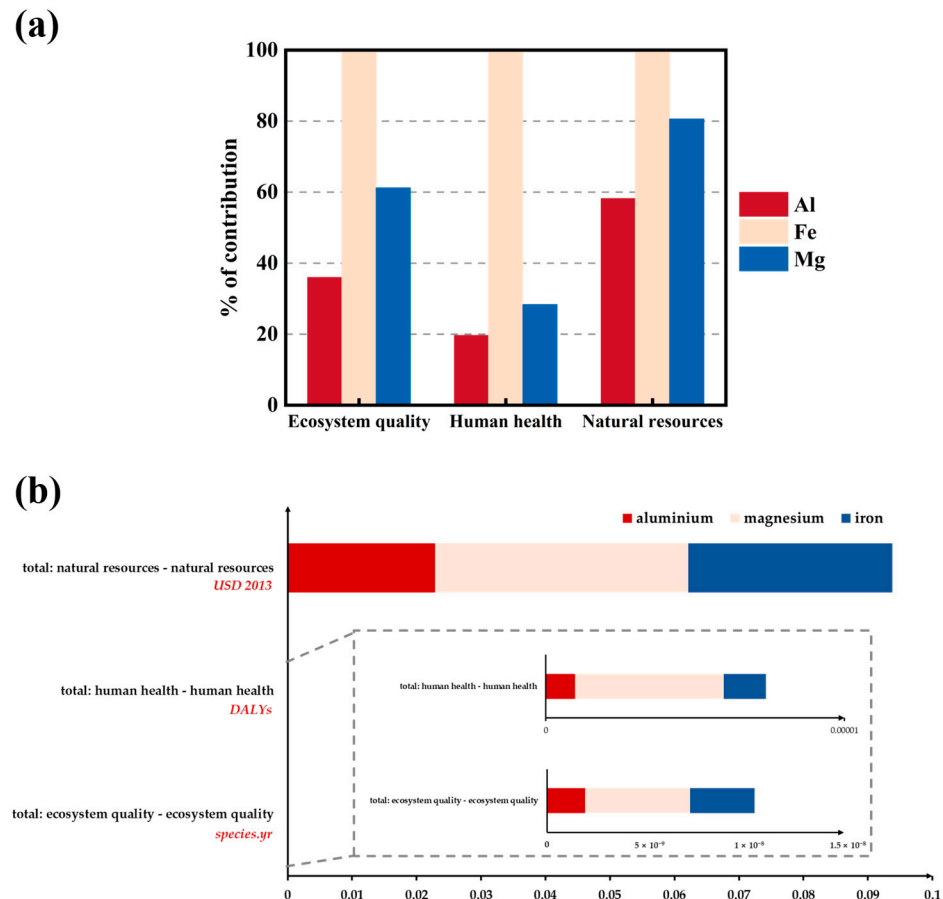


**Figure 14.** Analysis of the contribution of endpoint environmental impact indicators based on all scenarios: (a) results in percentages; (b) results in real values.

### 3.4.2. Sensitivity Analysis

Considering that the input parameters in the LCA are variable constants in terms of electrical energy and electrode mass, the variability of the input electrical energy is reflected in the possible current fluctuation in the stabilized power supply, and the variability of the electrode mass is reflected in the quality difference between different electrodes of the same material, both of which had an impact on the results of the LCA calculations. A sensitivity analysis was performed of the variable parameters based on the index of global warming in the LCA midpoint.

The formula for the sensitivity coefficient is provided for the case of a one-factor transformation:

$$S(y, x) = \frac{\Delta y / y}{\Delta x / x} \quad (11)$$

where, according to the definition of the derivative,  $S(y, x) = \frac{dy}{dx} \times \frac{x}{y}$  when  $\Delta x \rightarrow 0$ ,  $\Delta x$  is the amount of parameter changes,  $\Delta y$  is the changes in the results with the changes in the parameter,  $x$  is the initial value of the input parameter,  $y$  is the result computed under the initial conditions, and  $S$  is the sensitivity coefficient.

Under the condition of determining the input electrical energy and the mass of the electrode as the key parameters, the isolation of one variable at a time is used first to control the input mass of the three types of electrodes, to set the input electrical energy of the three types of materials under the condition of the initial data to change in magnitudes of  $\pm 1\%$ ,  $\pm 3\%$ , and  $\pm 5\%$ , and to determine the value of global warming in each condition. Then, this method is used to control the input electrical energy of the three types of electrodes, to set the mass of the three electrode materials to change by  $\pm 1\%$ ,  $\pm 3\%$ , and  $\pm 5\%$ , and to determine the value of global warming under each condition. The regression analysis method is utilized to fit the changing parameters and results and obtain the slope, and then the sensitivity coefficients can be determined.

The slopes obtained for the three electrode materials under controlled conditions with different variables are shown in Table 3.

**Table 3.** Slope of three electrode materials under control of different variable conditions.

	Al	Mg	Fe
Electricity	0.7222397	0.7222397	0.7222397
Mass	1.3235912	24.0822278	2.6650087

Considering the value of global warming as  $g$ , the mass of the electrode as  $m$ , and the input electric energy as  $e$ , there exists a relationship where  $g = f(m, e)$ ; when controlling the constant mass of the electrode,  $S(g, e) = \frac{dg}{de} \times \frac{e}{g}$ ; when controlling the endless input electrical energy and changing the mass of the electrode,  $S(g, m) = \frac{dg}{dm} \times \frac{m}{g}$ . The sensitivity coefficient can be easily derived from each condition according to the fitted slope, and a larger sensitivity coefficient indicates that the results are more sensitive to the parameter that is changed; that is, the change in the results caused by a slight change in the parameter is more prominent.

For the aluminum electrodes, the sum of the two sensitivity coefficients calculated from the two slopes was 1 under the condition of controlling the constant mass of the electrode, and similar results were obtained for the magnesium and iron electrodes. Under the initial value conditions, the sensitivity coefficient of the input electrical energy of the aluminum electrodes was 0.8873. The sensitivity coefficient of the electrode mass was 0.1117. With an increase in input electrical energy, the proportion of its sensitivity coefficient increased and the sensitivity coefficient became greater; that is, the magnitude of the change in global warming, calculated as carbon dioxide equivalent caused by a 1% change in each input electrical energy, becomes more extensive. Similar results were found for magnesium and iron electrodes, with iron showing the greatest increase in sensitivity coefficient among the three materials.

The sensitivity coefficients of the input electrical energy under the initial value conditions were observed to be 0.8873, 0.2731, and 0.05217 for aluminum, magnesium, and iron, respectively, indicating that for the aluminum electrode, the input electrical energy is a more critical parameter than the mass of the electrode. The calculation results are more sensitive to changes in the amount of electrical energy consumed. The results of the corresponding global warming for the magnesium electrodes showed that they are more susceptible to changes in electrode mass. In contrast, the iron electrodes showed similar sensitivities to the input electrical energy and electrode mass under the initial conditions.

Overall, the sensitivity coefficients of the three materials for the indicator of global warming were small ( $<1$ ). The magnitude of change in the results of the three materials under different variables is shown in Figure 15. The changes in the input electrical energy and mass of the electrode of the aluminum electrode are the straight lines with the largest and the smallest slopes, respectively. The magnitude of the change in the results of the two boundary lines is within 5%, which means that the change in the results of the other two materials was less than 5% under each variation condition. The magnitude of the change in the results was small, indicating that the LCA model is robust.

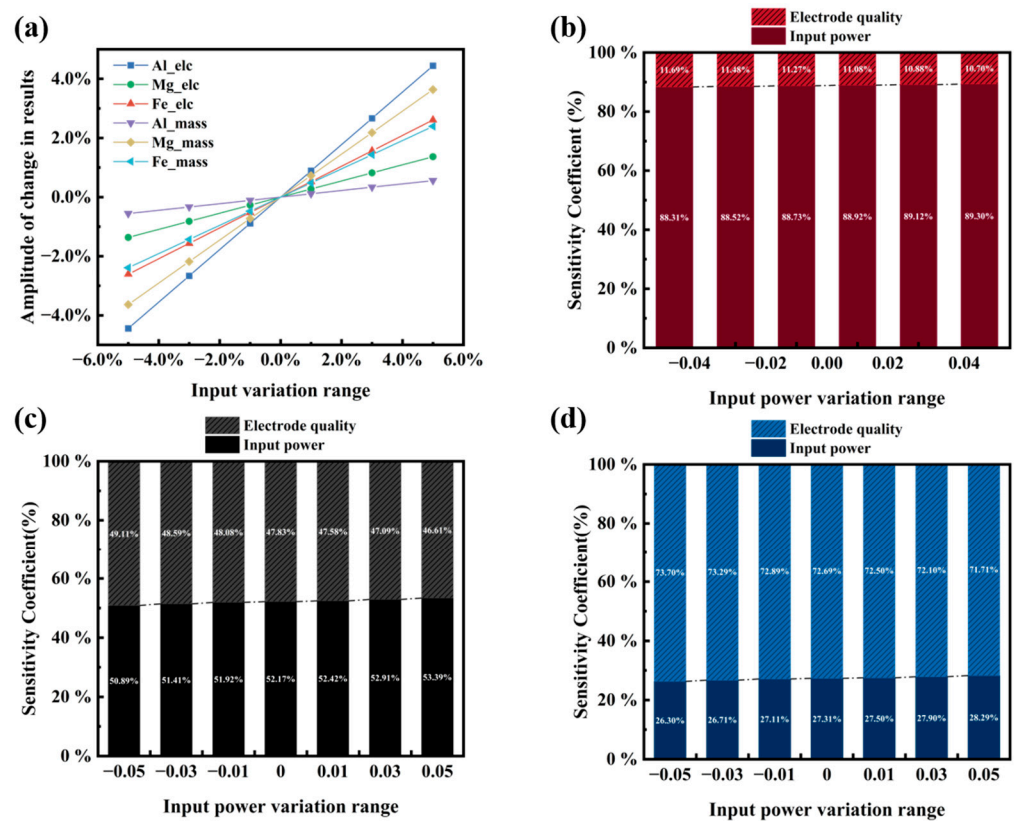


Figure 15. Sensitivity analysis: (a) Input variation range; (b–d) Input power variation range.

#### 4. Conclusions

This study examined the impacts of several anode materials (aluminum, iron, and magnesium) and operational parameters (ED, pH, and CD) on the effectiveness of removing phosphorus from simulated wastewater using electrocoagulation.

Through a comprehensive comparison, the aluminum electrode system showed the highest phosphate removal efficiency (90%) compared to that of the other two metals (iron, 80%; magnesium, 75%) and had the lowest energy consumption. Regarding the spacing of the electrodes, the mutual synergistic effect of air flotation and flocculation between the electrodes must be considered, and a suitable spacing was found for both the aluminum and magnesium electrode systems. However, the iron electrode system requires further exploration. Regarding the initial pH, the aluminum and iron electrode systems exhibited a better phosphate removal effect at a pH of 3 and better performance at a pH of 6. A magnesium electrode system should not have a neutral pH. With an increase in CD, the phosphate removal efficiency of the magnesium electrode gradually approached that of the aluminum and iron electrodes. Therefore, within the range of CDs studied, a CD of 6 mA/cm<sup>2</sup> is ideal for aluminum and iron electrode systems, whereas the magnesium electrode system requires a higher CD.

An analysis of the sludge using SEM, EDS, FT-IR, and XRD techniques demonstrated that electrocoagulation effectively removed phosphorus from the simulated wastewater.

Through economic analysis, after 20 min of energization, the aluminum and iron electrodes could achieve better removal efficiencies and maintain a particular economy, whereas the magnesium electrode system requires a greater energization time.

Three models, PFO, PSO, and BMG, were used to simulate the relationship between phosphate concentration and time in the three electrocoagulation systems for phosphate removal. We found that the fitting degrees of the three metal electrode systems for PFO and PSO were higher than that for the BMG model; however, the BMG model described the aluminum and iron electrode systems very well. In contrast, the fitting degree of the

magnesium electrodes was lower, and it is necessary to further study the magnesium electrode system for phosphorus removal.

The LCA revealed that the midpoint and endpoint environmental impacts were influenced by the type of anode material and water quality at the end of the treatment. Treatment with magnesium as the anode material led to the highest percentage contribution to all midpoint and endpoint indicators, except freshwater ecotoxicity. Therefore, the use of magnesium as a metal anode in this process is not recommended. Moreover, the use of aluminum led to a lower environmental impact than that of iron and magnesium in most midpoint and endpoint impact indicators. This should be considered when selecting anode materials for electrocoagulation of wastewater.

Therefore, electrocoagulation using aluminum electrodes is suitable for the pretreatment of phosphorus-containing wastewater and can be performed at a large scale.

In the future, we can harness the power of artificial intelligence and machine learning techniques to not only predict but also optimize the impact of critical operational parameters like electrode distance, pH, and current density. This approach offers significant advantages, enabling us to achieve a higher degree of precision and efficiency in phosphorus removal. By leveraging these techniques, we can fine-tune the operational conditions to maximize the effectiveness of the electrocoagulation process, leading to more sustainable and cost-effective wastewater treatment solutions. At the same time, this will also help us better achieve the United Nations Sustainable Development Goals (SDGs) and contribute to global environmental protection and sustainable development.

**Supplementary Materials:** The following supporting information can be downloaded at: <https://www.mdpi.com/article/10.3390/su16093836/s1>, Figure S1: SEM test results of three metal electroflocculation products: (a) aluminum, (b) iron, and (c) magnesium; Figure S2: EDS results of electrocoagulation products of aluminum metal electrode; Figure S3: EDS results of electrocoagulation products of iron metal electrodes; Figure S4: EDS results of electrocoagulation products of magnesium metal electrode; Figure S5: Analysis of the contribution of midpoint environmental impact indicators based on all scenarios. (Actual value.); Figure S6: Analysis of the contribution of endpoint environmental impact indicators based on all scenarios. (Actual value); Table S1: Goal and scope definition of this LCA study; Table S2: Cradle-to-grave LCA results of Scenario S1: functional unit = 1 m<sup>3</sup> simulated wastewater containing phosphorus; Table S3: Cradle-to-grave LCA results of Scenario 2: functional unit = 1 m<sup>3</sup> simulated wastewater containing phosphorus; Table S4: Cradle-to-grave LCA results of Scenario 3: functional unit = 1 m<sup>3</sup> simulated wastewater containing phosphorus; Table S5: Cradle-to-grave LCA results of comparison of scenarios 1–3: functional unit = 1 m<sup>3</sup> simulated wastewater containing phosphorus.

**Author Contributions:** Conceptualization, M.L.; methodology, Q.L.; software, W.Z.; validation, H.Z.; writing, G.L.; supervision, B.Z. All authors have read and agreed to the published version of the manuscript.

**Funding:** This research was funded by Engineering Technology Research Institute of Xinjiang Oilfield Company, grant number 20200023.

**Institutional Review Board Statement:** Not applicable.

**Informed Consent Statement:** Not applicable.

**Data Availability Statement:** All the data generated or analyzed during this study are included in this published article.

**Conflicts of Interest:** The authors declare no conflicts of interest.

## References

1. Wang, C.; Wang, C.; Xu, M.; Zhang, F. Phosphorus removal by iron–carbon microelectrolysis: A new way to achieve phosphorus recovery. *Green Process. Synth.* **2023**, *12*, 20228120. [[CrossRef](#)]
2. Zhao, H. Research progress on treatment of low phosphorus wastewater. *Environ. Prot. Chem. Ind.* **2023**, *43*, 292–297.
3. Wu, S.; Chen, W. The Mechanism and Calamitousness of Eutrophication. *J. Catastrophology* **2004**, *19*, 13–17.

4. Tong, S.; Zhao, Y.; Zhu, M.; Li, J.; Liu, S.; Chen, S. Current situation and research progress of slaughter and meat processing wastewater treatment. *Ind. Water Treat.* **2019**, *39*, 6–10.
5. Ng, M.; Dalhatou, S.; Wilson, J.; Kamdem, B.P.; Temitope, M.B.; Paumo, H.K.; Djelal, H.; Assadi, A.A.; Phuong, N.T.; Kane, A. Characterization of Slaughterhouse Wastewater and Development of Treatment Techniques: A Review. *Processes* **2022**, *10*, 1300. [[CrossRef](#)]
6. Chen, F.Y.; Wu, Z.Y.; Gupta, S.; Rivera, D.J.; Lambeets, S.V.; Pecaut, S.; Kim, J.Y.T.; Zhu, P.; Finprock, Y.Z.; Meira, D.M.; et al. Efficient conversion of low-concentration nitrate sources into ammonia on a Ru-dispersed Cu nanowire electrocatalyst. *Nat. Nanotechnol.* **2022**, *17*, 759–767. [[CrossRef](#)]
7. Yang, L.; Jiao, Y.; Xu, X.M.; Pan, Y.L.; Su, C.; Duan, X.G.; Sun, H.Q.; Liu, S.M.; Wang, S.B.; Shao, Z.P. Superstructures with Atomic-Level Arranged Perovskite and Oxide Layers for Advanced Oxidation with an Enhanced Non-Free Radical Pathway. *ACS Sustain. Chem. Eng.* **2022**, *10*, 1899–1909. [[CrossRef](#)]
8. Ma, Y.; Liu, Y.; Su, Y.; Li, G. Research progress on modified adsorbent applied in phosphorus removal from wastewater. *New Chem. Mater.* **2021**, *49*, 266–270.
9. Liu, R.T.; Sui, Y.M.; Wang, X.Z. Metal-organic framework-based ultrafiltration membrane separation with capacitive-type for enhanced phosphate removal. *Chem. Eng. J.* **2019**, *371*, 903–913. [[CrossRef](#)]
10. Unuabonah, E.I.; Agunbiade, F.O.; Alfred, M.O.; Adewumi, T.A.; Okoli, C.P.; Omorogie, M.O.; Akanbi, M.O.; Ofomaja, A.E.; Taubert, A. Facile synthesis of new amino-functionalized agrogenic hybrid composite clay adsorbents for phosphate capture and recovery from water. *J. Clean. Prod.* **2017**, *164*, 652–663. [[CrossRef](#)]
11. Zhang, H.L.; Elskens, M.; Chen, G.X.; Chou, L. Phosphate adsorption on hydrous ferric oxide (HFO) at different salinities and pHs. *Chemosphere* **2019**, *225*, 352–359. [[CrossRef](#)]
12. Vikrant, K.; Kim, K.H.; Ok, Y.S.; Tsang, D.C.W.; Tsang, Y.F.; Giri, B.S.; Singh, R.S. Engineered/designer biochar for the removal of phosphate in water and wastewater. *Sci. Total Environ.* **2018**, *616*, 1242–1260. [[CrossRef](#)]
13. Cui, H.J.; Cai, J.K.; Zhao, H.; Yuan, B.L.; Ai, C.L.; Fu, M.L. Fabrication of magnetic porous Fe-Mn binary oxide nanowires with superior capability for removal of As(III) from water. *J. Hazard. Mater.* **2014**, *279*, 26–31. [[CrossRef](#)]
14. Bacelo, H.; Pintor, A.M.A.; Santos, S.C.R.; Boaventura, R.A.R.; Botelho, C.M.S. Performance and prospects of different adsorbents for phosphorus uptake and recovery from water. *Chem. Eng. J.* **2020**, *381*, 122566. [[CrossRef](#)]
15. Xie, Y.; Chen, R.; Tao, Z.; Jing, Z. Progress in enhanced phosphorus removal from sanitary sewage. *Appl. Chem. Ind.* **2021**, *50*, 821–824.
16. Qian, J.; Song, L.; Zhang, D.; Xu, D.; Xie, Z. The buried wastewater treatment plant in Zhouzhuang Ancient Town. *J. Hefei Polytech. Univ. Nat. Ed.* **2005**, *28*, 940–943.
17. Guo, L.; Chen, Y.; Liu, C.; Shang, H.; Li, C. Recovery of concentrated ammoniacal nitrogen from rare earth ammonium sulfate wastewater by magnesium ammonium sulfate precipitation method. *Mod. Chem. Ind.* **2018**, *38*, 73–76+78.
18. Song, X.; Ren, T.; Ma, C.; Bai, J.; Lin, L. Research progress of chemical agents on technology of removal phosphorus in urban sewage treatment plants. *Appl. Chem. Ind.* **2020**, *49*, 2056–2057+2062.
19. Hou, J.L.; Yong, K. Research progress of biological removal of nitrogen and phosphorus in municipal sewage. *Chem. Ind. Eng. Prog.* **2007**, *26*, 366–370+376.
20. Mao, Y.L.; Xiong, R.W.; Gao, X.F.; Jiang, L.; Peng, Y.C.; Xue, Y. Analysis of the Status and Improvement of Microalgal Phosphorus Removal from Municipal Wastewater. *Processes* **2021**, *9*, 1486. [[CrossRef](#)]
21. Zhang, F.; Chen, X.; Jiang, Z.; Wang, L.; He, Y.; Bao, Z. Growth characteristics and removal efficiency of nitrogen and phosphorus of two kinds of non-toxic microalgae under different nitrogen and phosphorus concentrations. *Chin. J. Environ. Eng.* **2015**, *9*, 559–566.
22. Hellal, M.S.; Doma, H.S.; Abou-Taleb, E.M. Techno-economic evaluation of electrocoagulation for cattle slaughterhouse wastewater treatment using aluminum electrodes in batch and continuous experiment. *Sustain. Environ. Res.* **2023**, *33*, 2. [[CrossRef](#)]
23. Potrich, M.C.; Duarte, E.d.S.A.; Sikora, M.d.S.; Costa da Rocha, R.D. Electrocoagulation for nutrients removal in the slaughterhouse wastewater: Comparison between iron and aluminum electrodes treatment. *Environ. Technol.* **2022**, *43*, 751–765. [[CrossRef](#)]
24. Zhu, H. Research Progress of Electrocoagulation Integration Technology and Application. *Technol. Water Treat.* **2023**, *49*, 7–10+33.
25. Hakizimana, J.N.; Gourich, B.; Chafi, M.; Stiriba, Y.; Vial, C.; Drogui, P.; Naja, J. Electrocoagulation process in water treatment: A review of electrocoagulation modeling approaches. *Desalination* **2017**, *404*, 1–21. [[CrossRef](#)]
26. Li, J.H.; Bai, J.; Huang, K.; Zhou, B.X.; Wang, Y.H.; Hu, X.F. Removal of trivalent chromium in the complex state of trivalent chromium passivation wastewater. *Chem. Eng. J.* **2014**, *236*, 59–65. [[CrossRef](#)]
27. Durante, C.; Cuscov, M.; Isse, A.A.; Sandonà, G.; Gennaro, A. Advanced oxidation processes coupled with electrocoagulation for the exhaustive abatement of Cr-EDTA. *Water Res.* **2011**, *45*, 2122–2130. [[CrossRef](#)]
28. An, C.J.; Huang, G.; Yao, Y.; Zhao, S. Emerging usage of electrocoagulation technology for oil removal from wastewater: A review. *Sci. Total Environ.* **2017**, *579*, 537–556. [[CrossRef](#)]
29. Akarsu, C.; Bilici, Z.; Dizge, N. Treatment of vegetable oil wastewater by a conventional activated sludge process coupled with electrocoagulation process. *Water Environ. Res.* **2022**, *94*, e10692. [[CrossRef](#)]
30. Sandi; Afriani, F.; Tiandho, Y. Application of electrocoagulation for textile wastewater treatment: A review. In Proceedings of the 2nd International Conference on Green Energy and Environment (ICoGEE), Bangka Belitung Islands, Indonesia, 8 October 2020; IOP Science: Bristol, UK, 2020.

31. Yánes, A.; Pinedo-Hernández, J.; Marrugo-Negrete, J. Continuous Flow Electrocoagulation as a Hospital Wastewater Treatment. *Port. Electrochim. Acta* **2021**, *39*, 403–413. [[CrossRef](#)]
32. Eryuruk, K.; Un, U.T.; Ogutveren, U.B. Electrochemical treatment of wastewaters from poultry slaughtering and processing by using iron electrodes. *J. Clean. Prod.* **2018**, *172*, 1089–1095. [[CrossRef](#)]
33. Shi, S. Experimental study of slaughterhouse wastewater treatment with reverse pulse electrocoagulation. *Technol. Water Treat.* **2010**, *36*, 104–107.
34. Tanatti, N.P.; Sezer, M. Optimizing electrocoagulation for poultry slaughterhouse wastewater treatment: A fuzzy axiomatic design approach. *Environ. Sci. Pollut. Res.* **2024**. [[CrossRef](#)]
35. Teng, W.W.; Liu, S.J.; Zhang, X.; Zhang, F.; Yang, X.L.; Xu, M.X.; Hou, J.W. Reliability Treatment of Silicon in Oilfield Wastewater by Electrocoagulation. *Water* **2023**, *15*, 206. [[CrossRef](#)]
36. Liu, M.H.; Ma, S.; Wang, X.; Wang, M.M.; Zhao, Y.T.; Yan, Z.P.; Wang, E.R.; Zhang, H.; Xue, T.Y. Effective removal of dissolved silica from white carbon black wastewater by iron electrode electrocoagulation: Process optimization and simulation. *J. Water Process Eng.* **2022**, *47*, 102812. [[CrossRef](#)]
37. Omwene, P.I.; Koby, M.; Can, O.T. Phosphorus removal from domestic wastewater in electrocoagulation reactor using aluminium and iron plate hybrid anodes. *Ecol. Eng.* **2018**, *123*, 65–73. [[CrossRef](#)]
38. Supriya, V.; Sohan Joshua, M.; Ram Kiran, B.; Guduru, N.; Rao Poiba, V.; Vangalapati, M. Investigation of experimental parameters and It's optimization on iron plate electrodes for the removal of phosphates by electrocoagulation process using Box–Behnken design. *Mater. Today Proc.* **2023**, *in press*. [[CrossRef](#)]
39. Dura, A.; Breslin, C.B. The removal of phosphates using electrocoagulation with Al–Mg anodes. *J. Electroanal. Chem.* **2019**, *846*, 113161. [[CrossRef](#)]
40. Devlin, T.R.; Kowalski, M.S.; Pagaduan, E.; Zhang, X.; Wei, V.; Oleszkiewicz, J.A. Electrocoagulation of wastewater using aluminum, iron, and magnesium electrodes. *J. Hazard. Mater.* **2019**, *368*, 862–868. [[CrossRef](#)] [[PubMed](#)]
41. Omwene, P.I.; Koby, M. Treatment of domestic wastewater phosphate by electrocoagulation using Fe and Al electrodes: A comparative study. *Process Saf. Environ. Prot.* **2018**, *116*, 34–51. [[CrossRef](#)]
42. Bhoi, G.P.; Singh, K.S.; Connor, D.A. Optimization of phosphorus recovery using electrochemical struvite precipitation and comparison with iron electrocoagulation system. *Water Environ. Res.* **2023**, *95*, e10847. [[CrossRef](#)]
43. Zaffar, A.; Krishnamoorthy, N.; Nagaraj, N.; Jayaraman, S.; Paramasivan, B. Optimization and kinetic modeling of phosphate recovery as struvite by electrocoagulation from source-separated urine. *Environ. Sci. Pollut. Res.* **2023**, *30*, 20721–20735. [[CrossRef](#)] [[PubMed](#)]
44. García-Orozco, V.M.; Barrera-Díaz, C.E.; Roa-Morales, G.; Linares-Hernández, I. A Comparative Electrochemical-Ozone Treatment for Removal of Phenolphthalein. *J. Chem.* **2016**, *2016*, 8105128. [[CrossRef](#)]
45. Safwat, S.M.; Mohamed, N.Y.; El-Seddik, M.M. Performance evaluation and life cycle assessment of electrocoagulation process for manganese removal from wastewater using titanium electrodes. *J. Environ. Manag.* **2023**, *328*, 116967. [[CrossRef](#)] [[PubMed](#)]
46. da Costa, E.P.; Bottrel, S.E.C.; Starling, M.; Leao, M.M.D.; Amorim, C.C. Degradation of carbendazim in water via photo-Fenton in Raceway Pond Reactor: Assessment of acute toxicity and transformation products. *Environ. Sci. Pollut. Res.* **2019**, *26*, 4324–4336. [[CrossRef](#)] [[PubMed](#)]
47. *ISO 14044; Environmental Management—Life Cycle Assessment—Requirements and Guidelines*. International Organization for Standardization: Geneva, Switzerland, 2006.
48. Amri, I.; Herman, S.; Ramadan, A.F.; Hamzah, N. Effect of electrode and electric current on peat water treatment with continuous electrocoagulation process. In Proceedings of the 2nd International Conference on Chemical Engineering and Applied Sciences (ICChEAS), Semarang, Indonesia, 3–4 November 2021; pp. S520–S525.
49. Wu, Y.; Zhang, P.; Lu, J.; Xu, H.; Zhang, W.; Yu, W.; Jiang, G. Fe electrocoagulation technology for effective removal of molybdate from water: Main influencing factors, response surface optimization, and mechanistic analysis. *J. Environ. Chem. Eng.* **2024**, *12*, 112127. [[CrossRef](#)]
50. Weiss, S.F.; Christensen, M.L.; Jorgensen, M.K. Mechanisms behind pH changes during electrocoagulation. *Aiche J.* **2021**, *67*, e17384. [[CrossRef](#)]
51. Attour, A.; Touati, M.; Thin, M.; Ben Amor, M.; Lopicque, F.; Leclerc, J.P. Influence of operating parameters on phosphate removal from water by electrocoagulation using aluminum electrodes. *Sep. Purif. Technol.* **2014**, *123*, 124–129. [[CrossRef](#)]
52. Mithra, S.S.; Ramesh, S.T.; Gandhimathi, R.; Nidheesh, P.V. Studies on the removal of phosphate from water by electrocoagulation with aluminium plate electrodes. *Environ. Eng. Manag. J.* **2017**, *16*, 2293–2301.
53. He, C.C.; Hu, C.Y.; Lo, S.L. Integrating chloride addition and ultrasonic processing with electrocoagulation to remove passivation layers and enhance phosphate removal. *Sep. Purif. Technol.* **2018**, *201*, 148–155. [[CrossRef](#)]
54. Carmona-Carmona, P.F.; Linares-Hernández, I.; Teutli-Sequeira, E.A.; López-Rebollar, B.M.; Alvarez-Bastida, C.; Mier-Quiroga, M.D.; Vázquez-Mejía, G.; Martínez-Miranda, V. Industrial wastewater treatment using magnesium electrocoagulation in batch and continuous mode. *J. Environ. Sci. Health Part A-Toxic/Hazard. Subst. Environ. Eng.* **2020**, *56*, 269–288. [[CrossRef](#)]
55. Chen, P.; Li, J.F.; Xie, N.N. Study on Influencing Parameters of Total Phosphorus Degradation in Cattle Farm Wastewater by Electrocoagulation Using Magnesium, Aluminum, and Iron Electrodes. *Water* **2023**, *15*, 4134. [[CrossRef](#)]

56. Garcia-Orozco, V.M.; Linares-Hernandez, I.; Natividad, R.; Balderas-Hernandez, P.; Alanis-Ramirez, C.; Barrera-Diaz, C.E.; Roa-Morales, G. Solar-photovoltaic electrocoagulation of wastewater from a chocolate manufacturing industry: Anodic material effect (aluminium, copper and zinc) and life cycle assessment. *J. Environ. Chem. Eng.* **2022**, *10*, 107969. [[CrossRef](#)]
57. Tan, K.L.; Hameed, B.H. Insight into the adsorption kinetics models for the removal of contaminants from aqueous solutions. *J. Taiwan Inst. Chem. Eng.* **2017**, *74*, 25–48. [[CrossRef](#)]
58. Xue, M.X.; Kang, X.S.; Wang, Y.; Gao, B.Y. Comparison of aluminum formate and traditional aluminum coagulants in structure, hydrolysates, coagulation behavior, and its corrosion resistance advantage. *Sep. Purif. Technol.* **2024**, *335*, 126065. [[CrossRef](#)]
59. Ferreira, A.D.; Queiroz, H.M.; Otero, X.L.; Barcellos, D.; Bernardino, A.F.; Ferreira, T.O. Iron hazard in an impacted estuary: Contrasting controls of plants and implications to phytoremediation. *J. Hazard. Mater.* **2022**, *428*, 128216. [[CrossRef](#)] [[PubMed](#)]
60. Park, H.; Nam, K.; Lee, J. Lessons from aluminum and magnesium scraps fires and explosions: Case studies of metal recycling industry. *J. Loss Prev. Process Ind.* **2022**, *80*, 104872. [[CrossRef](#)]
61. Paraschiv, S.; Paraschiv, L.S. Trends of carbon dioxide (CO<sub>2</sub>) emissions from fossil fuels combustion (coal, gas and oil) in the EU member states from 1960 to 2018. *Energy Rep.* **2020**, *6*, 237–242. [[CrossRef](#)]
62. Baz, K.; Xu, D.Y.; Ali, H.; Khan, U.; Cheng, J.H.; Abbas, K.; Ali, I. Nexus of minerals-technology complexity and fossil fuels with carbon dioxide emission: Emerging Asian economies based on product complexity index. *J. Clean. Prod.* **2022**, *373*, 133703. [[CrossRef](#)]
63. Madkour, L.H. Heavy metals and free radical-induced cell death mechanisms. In *Reactive Oxygen Species (ROS), Nanoparticles, and Endoplasmic Reticulum (ER) Stress-Induced Cell Death Mechanisms*; Elsevier Science: Amsterdam, The Netherlands, 2020.
64. Mohankumar, T.; Venugopal, D.; Palaniyappan, J.; Beerappa, R.; Duraisamy, E.; Velu, S. 3—Environmental exposure to heavy metals in ambient air and its human health implications. In *Spatial Modeling of Environmental Pollution and Ecological Risk*; Shit, P.K., Datta, D.K., Bera, B., Islam, A., Adhikary, P.P., Eds.; Woodhead Publishing: Sawston, UK, 2024; pp. 41–69.
65. Liu, J.; Zhao, J.; Du, J.; Peng, S.; Wu, J.; Zhang, W.; Yan, X.; Lin, Z. Predicting the binding configuration and release potential of heavy metals on iron (oxyhydr)oxides: A machine learning study on EXAFS. *J. Hazard. Mater.* **2024**, *468*, 133797. [[CrossRef](#)]
66. Xie, Y.; Mao, Y.; Zhong, P.; Zhang, Y.; Zhang, L.; Chen, W.; Qu, C.; Xing, X.; Cao, J.; Zhang, J. Seasonal variations and size-dependent distribution of heavy metals in particulate matter in Huangshi: Implications for human health risk assessment. *Atmos. Environ.* **2024**, *322*, 120384. [[CrossRef](#)]
67. Li, Z.; Yang, D.W.; Li, S.S.; Yang, L.; Yan, W.; Xu, H. Advances on electrochemical disinfection research: Mechanisms, influencing factors and applications. *Sci. Total Environ.* **2024**, *912*, 169043. [[CrossRef](#)] [[PubMed](#)]
68. Priyanka, P.; Srivastava, N.; Chattopadhyay, J. Chapter 5—Analysis of complex microbial communities in soil and wastewater treatment processes. In *Functional Metagenomics*; Shah, M.P., Ed.; Academic Press: Cambridge, MA, USA, 2024; pp. 131–142.

**Disclaimer/Publisher’s Note:** The statements, opinions and data contained in all publications are solely those of the individual author(s) and contributor(s) and not of MDPI and/or the editor(s). MDPI and/or the editor(s) disclaim responsibility for any injury to people or property resulting from any ideas, methods, instructions or products referred to in the content.